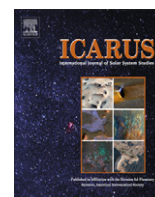




Contents lists available at ScienceDirect

Icarus

journal homepage: [www.elsevier.com/locate/icarus](http://www.elsevier.com/locate/icarus)

## The influence of mantle melting on the evolution of Mars

Abigail A. Fraeman<sup>1</sup>, Jun Korenaga<sup>\*</sup>

Department of Geology and Geophysics, Yale University, New Haven, CT 06520, USA

### ARTICLE INFO

#### Article history:

Received 28 October 2009

Revised 16 June 2010

Accepted 21 June 2010

Available online 30 June 2010

#### Keywords:

Mars, Interior  
Thermal histories  
Mars, Surface

### ABSTRACT

We present a parameterized convection model of Mars by incorporating a new heat-flow scaling law for stagnant-lid convection, to better understand how the evolution of Mars may be affected by mantle melting. Melting in the mantle during convection leads to the formation of a compositionally buoyant lithosphere, which may also be intrinsically more viscous by dehydration. The consequences of these melting effects on the evolution of terrestrial planets have not been explored before. The temporal evolution of crust and lithospheric mantle is modeled in a self-consistent manner considering mantle melting, convective instability, and the rewetting of dehydrated lithosphere from below by hydrogen diffusion. Though the effect of compositional buoyancy turns out to be minimal, the introduction of viscosity contrast between wet and dry mantle can considerably slow mantle cooling and sometimes lead to non-monotonic core cooling. Furthermore, with or without dehydration stiffening, our model predicts that the martian mantle must have been degassed more extensively (>80%) than previously suggested (<10%); the loss of such a large amount of water from the mantle to surface has significant implications about the role of water in the early surface and climate evolution of Mars.

© 2010 Elsevier Inc. All rights reserved.

### 1. Introduction

The thermal history of a terrestrial planet places a first-order control on the physical and chemical evolution of the planet, and there have been a large number of theoretical studies attempting to reconstruct how terrestrial planets have been cooling since their formation (e.g., Stevenson et al., 1983; Spohn, 1991; Solomatov and Moresi, 1996; Hauck and Phillips, 2002). The primary cooling mechanism of such planets is believed to be some form of thermal convection in the mantle, and convective upwelling results in partial melting if the mantle is sufficiently hot. The crustal layer at the surface, which is most accessible by planetary investigation, could be produced largely by this endogenous chemical differentiation of the mantle.

Planetary cooling thus drives crustal evolution through mantle convection, but the evolution of the crust, or more generally the partial melting of the mantle, can in turn affect how a planet cools. First, partial melting extracts incompatible heat-producing elements such as U and Th from the convecting mantle and sequesters them in the crust. A crust enriched with heat-producing elements may become hot enough to insulate the underlying mantle from surface cooling (e.g., Phillips and Malin, 1983). Second, the residual mantle after the extraction of partial melt tends to be less dense

than the unmelted mantle, and this chemically buoyant material could influence the growth of the top thermal boundary layer. The competition between positive compositional buoyancy and negative thermal buoyancy may cause the boundary layer to become unstable and undergo alternating periods of accumulation and delamination over a substantial portion of planetary evolution (Parmentier and Hess, 1992). Third, the residual mantle is also devoid of water because hydrogen is efficiently partitioned into the liquid phase, and this dehydration is known to result in a significant increase in the viscosity of the residual mantle (Karato et al., 1986; Hirth and Kohlstedt, 1996). Dehydration stiffening can also influence the nature of compositional buoyancy effects by stabilizing the growth of the top thermal boundary layer (Korenaga and Jordan, 2002b). Likely scenarios for planetary accretion suggest that the planetary mantle could have initially been moderately wet like Earth's oceanic upper mantle (i.e., a few hundred ppm H/Si) (e.g., Wänke and Dreibus, 1994; Lunine et al., 2003), so dehydration upon melting would be important until water in the mantle is exhausted.

Though the combination of compositional buoyancy and dehydration stiffening has been suggested to affect mantle dynamics in a significant way (Korenaga, 2003), previous studies are limited to modeling these effects in the dynamics of plate-tectonic convection (Korenaga, 2006, 2008), which is applicable to Earth, but not generally to other terrestrial planets. The influence of such melting-induced effects on more relevant stagnant-lid convection has been quantified only recently (Korenaga, 2009b), and the preliminary analysis suggests that mantle melting could reduce surface

<sup>\*</sup> Corresponding author. Fax: +1 203 432 3134.

E-mail address: [jun.korenaga@yale.edu](mailto:jun.korenaga@yale.edu) (J. Korenaga).

<sup>1</sup> Present address: Department of Earth and Planetary Sciences, Washington University, St. Louis, MO 63130, USA

heat flux by up to a factor of  $\sim 5$ – $10$  with respect to predictions based on the conventional scaling of stagnant-lid convection (e.g., Solomatov and Moresi, 2000). This degree of reduction may modify predictions from thermal evolution models rather drastically. The thermal evolution of a planet depends on a large number of model parameters, however, so the true significance of the melting effects is difficult to assess without actually embedding them into the modeling of thermal evolution.

The purpose of this paper is to model the thermal and chemical evolution of a terrestrial planet by taking into account the effects of mantle melting in a self-consistent manner. Here we focus on Mars for the following three reasons: (1) the effects of mantle melting are expected to be more significant for smaller planets because lower gravity (i.e., lower pressure) means melting starts at a greater depth if compared at the same temperature; (2) low pressures on Mars mean that the bulk of the martian mantle acts in a similar fashion to Earth's upper mantle, the rheology of which is much better characterized than that of the lower mantle; and (3) Mars has frequently been the target of planetary exploration in recent years and will likely continue to be so, thereby allowing various predictions from this study to be tested by observations.

## 2. Theoretical formulation

Our theoretical formulation follows the parameterized convection model of Stevenson et al. (1983) with the modification of Hauck and Phillips (2002) to account for coupled crust-magmatic evolution. In order to incorporate the new heat-flow scaling law of Korenaga (2009b), some additional parameters are introduced to track the chemical evolution of the mantle lithosphere and the convecting mantle. The details of formulation are given in the following subsections with an emphasis on what differs from previous studies.

Many previous studies on the thermal evolution of Mars employ the following two major assumptions, which are also adopted here. First, we assume that the mineralogical composition of the martian mantle is similar to that of Earth's mantle. The composition of the martian mantle is poorly constrained owing to the lack of direct mantle samples. Existing estimates are based on the compositions of martian meteorites and models of the planet's density distribution with depth (e.g., Dreibus and Wänke, 1985; Bertka and Fei, 1998; Sanloup et al., 1999; Khan and Connolly, 2008). These estimates predict that the mineralogy of the martian mantle is dominated either by olivine (e.g., Dreibus and Wänke, 1985) or by pyroxene (e.g., Sanloup et al., 1999). Earth's mantle is an olivine-dominated system, and its melting behavior is much better understood than that of the pyroxene-dominated system thanks to numerous petrological studies (e.g., McKenzie and Bickle, 1988; Langmuir et al., 1992; Walter, 1998; Herzberg et al., 2007). Additionally, whereas water has been shown to have a strong influence on the rheology of olivine-dominated system (Chopra and Paterson, 1984; Karato et al., 1986; Mei and Kohlstedt, 2000a,b), its role in a pyroxene-dominated system is less clear. We assume an Earth-like composition for the martian mantle because it allows us to parameterize its melting behavior with some confidence. Our theoretical formulation itself is independent of the mineralogical assumption, however, so our model can easily be adjusted for the pyroxene-dominated system if sufficient experimental data become available in the future.

Second, we assume that the martian mantle convects in the mode of stagnant-lid convection throughout its entire history. In stagnant-lid convection, convection takes place only beneath an immobile rigid plate, which covers the entire surface of a planet. This regime is commonly believed to be operating at present in the mantle of terrestrial planets other than Earth (e.g., Schubert

et al., 2001). The possibility of plate-tectonic convection in the past, in which surface plates are recycled back into the mantle, has been suggested for Mars to explain the origin of the hemispheric dichotomy (Sleep, 1994). Magnetic lineations on Mars resembling those at seafloor spreading were reported as potential evidence for plate tectonics (Connerney et al., 1999), whereas Fairén et al. (2002) claim that these lineations were formed through accretion of terranes. The influence of early plate tectonics on thermal evolution has also been explored (Nimmo and Stevenson, 2000; Breuer and Spohn, 2003). The hemispheric dichotomy of Mars, however, does not necessarily require a different mode of convection to form and other potential formation mechanisms such as a bolide impact have gained popularity in recent years (Marinova et al., 2008; Nimmo et al., 2008). Stagnant-lid convection is the most natural mode of thermal convection due to the strongly temperature-dependent rheology of silicate rocks (Solomatov, 1995), and other weakening mechanisms, which are still poorly understood, are necessary for plate tectonics to begin (e.g., Bercovici, 2003; Korenaga, 2007). Thermal evolution with stagnant-lid convection therefore serves as a reference for this study, upon which we can later impose other complications if necessary.

### 2.1. Governing equations

The governing equations in our parameterized convection model are the following energy balance for the mantle and the core. The energy balance for the mantle may be expressed as (Hauck and Phillips, 2002):

$$\frac{4}{3}\pi(R_m^3 - R_c^3)\left(Q_m - \rho_m c_m \eta_m \frac{dT_u}{dt}\right) - \rho_m f_m L_m = 4\pi(R_m^2 F_m - R_c^2 F_c), \quad (1)$$

where  $R_m$  and  $R_c$  are the radii of the mantle and the core, respectively,  $Q_m$  is heat production per unit volume in the mantle,  $\rho_m$  and  $c_m$  are the average density and specific heat of the mantle,  $\eta_m$  is a constant relating the upper mantle temperature (or equivalently, mantle potential temperature),  $T_u$ , to the average mantle temperature,  $f_m$  is volumetric melt production,  $L_m$  is latent heat released during melting, and  $F_m$  and  $F_c$  are heat fluxes across the mantle-crust boundary and the core-mantle boundary, respectively. Similarly, the core energy balance may be given as (Stevenson et al., 1983):

$$\left\{4\pi R_i^2 \rho_c (L_c + E_g) \frac{dR_i}{dT_{cm}} - \frac{4}{3}\pi R_c^3 \rho_c c_c \eta_c\right\} \frac{dT_{cm}}{dt} = 4\pi R_c^2 F_c, \quad (2)$$

where  $R_i$  is the radius of the inner core,  $L_c$  is the latent heat of solidification due to the growth of the inner core,  $E_g$  is the gravitational energy made available per unit mass of inner core material,  $T_{cm}$  is the core-side temperature at the core-mantle boundary,  $\eta_c$  is a constant relating  $T_{cm}$  to the average core temperature, and  $\rho_c$  and  $c_c$  are the average density and specific heat of the core, respectively. Some parameters such as  $R_c$ ,  $\rho_m$ , and  $c_m$  are constant, but many others are time-varying and often related to mantle melting. Key model constants are summarized in Table 1 with values adopted in this study.

Our treatment of core cooling (Eq. (2)) is identical to that of Stevenson et al. (1983), including the parameterization of the core heat flux  $F_c$ . The novel features of this study all regard solving the mantle energy balance of Eq. (1) taking into account various effects of mantle melting on both crustal and mantle evolution (Fig. 1). The heat production in the mantle  $Q_m$  decreases with time not only by radiogenic decay but also by extraction due to melting. The mantle radius  $R_m$  is identical to the radius of the planet  $R_p$  at the beginning but decreases as the crustal layer thickens. The rate of mantle melting  $f_m$  is controlled by the potential temperature  $T_u$

**Table 1**  
List of key model constants.

Parameter	Definition	Value	Unit	Reference
$g$	Gravitational acceleration	3.7	$\text{m s}^{-2}$	[1]
$T_s$	Surface temperature	220	K	[2]
$\eta_m$	Ratio of average and potential $T$ in the mantle	1.0	–	[1]
$\eta_c$	Ratio of average and potential $T$ in the core	1.1	–	[1]
$R_p$	Planet radius	$3390 \times 10^3$	m	[3]
$R_c$	Core radius	$1550 \times 10^3$	m	[3]
$\rho_m$	Mantle density	3527	$\text{kg m}^{-3}$	[3]
$\rho_c$	Core density	7200	$\text{kg m}^{-3}$	[3]
$c_m$	Specific heat of the mantle	1149	$\text{J K}^{-1} \text{kg}^{-1}$	[3]
$c_c$	Specific heat of the core	571	$\text{J K}^{-1} \text{kg}^{-1}$	[3]
$\lambda$	Radiogenic decay constant	$1.38 \times 10^{-17}$	$\text{s}^{-1}$	[1]
$\alpha_m$	Thermal expansivity of the mantle	$2 \times 10^{-5}$	$\text{K}^{-1}$	[1]
$k_m$	Thermal conductivity of the mantle	4	$\text{W K}^{-1} \text{m}^{-1}$	[1]
$\kappa_m$	Thermal diffusivity of the mantle	$10^{-6}$	$\text{m}^2 \text{s}^{-1}$	[1]
$L_m$	Latent heat of mantle melting	$600 \times 10^3$	$\text{J kg}^{-1}$	[3]
$L_c$	Latent heat of core solidification	$250 \times 10^3$	$\text{J kg}^{-1}$	[2]
$E_g$	Core gravitational energy release	$250 \times 10^3$	$\text{J kg}^{-1}$	[2]
$(dT/dP)_s$	Adiabatic gradient in the mantle	$1.54 \times 10^{-8}$	$\text{K Pa}^{-1}$	[4]
$(d\phi/dP)_s$	Melt productivity by adiabatic decompression	$0.12 \times 10^{-9}$	$\text{Pa}^{-1}$	[4]
$(d\rho/d\phi)$	Mantle density change by melting	–120	$\text{kg m}^{-3}$	[5]

References: 1. Stevenson et al. (1983), 2. Spohn (1991), 3. Hauck and Phillips (2002), 4. Korenaga et al. (2002c), and 5. Korenaga (2009b).

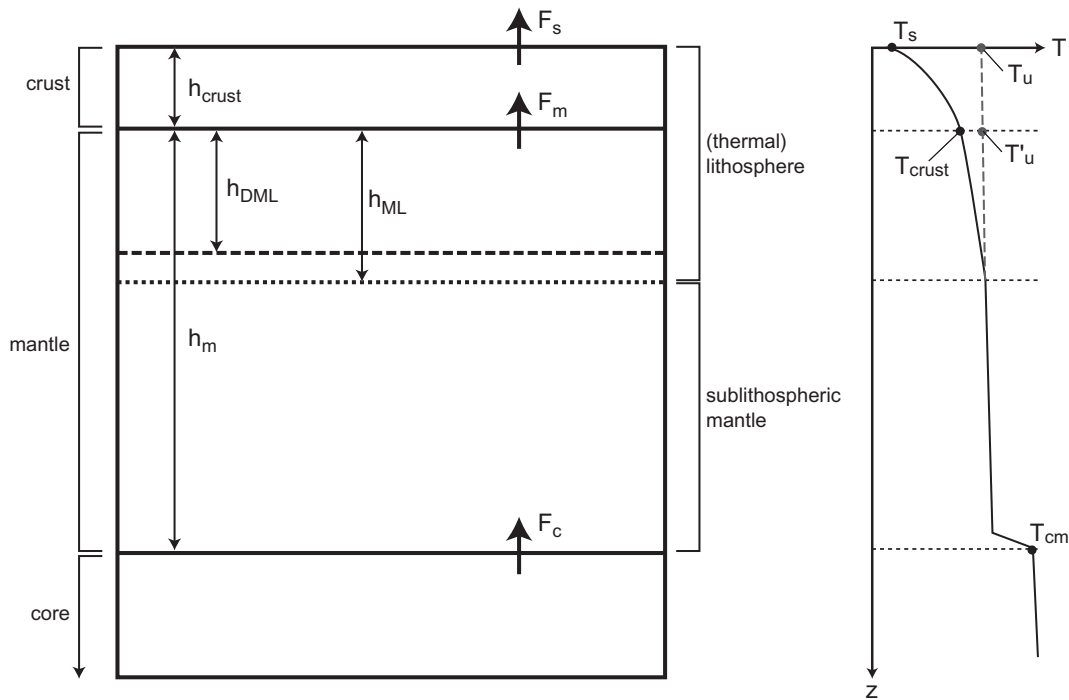


**Fig. 1.** Cartoons illustrating key model parameters relevant to the evolution of martian crust and mantle. Mars is divided into three chemically distinct layers: the crust, the mantle, and the core. The top thermal boundary layer, which is equivalent to (thermal) lithosphere, contains the entire crust and part of the mantle (mantle lithosphere, ML). The mantle beneath the lithosphere is sublithospheric mantle. The part of the mantle that has been processed by melting and stays in the thermal boundary layer is called depleted mantle lithosphere (DML). The left panel illustrates these various layers, and the right panel shows the corresponding (horizontally-averaged) temperature profile. In the left panel, the base of the depleted mantle lithosphere is shallower than the base of the stagnant lid (thermal lithosphere), and this situation corresponds to later times in the martian history when the sublithospheric mantle is too cold to melt. When the depleted mantle lithosphere is growing due to mantle melting, its base coincides with the (predicted) base of the stagnant lid if the depleted lithosphere has high enough viscosity. If not, part of the depleted lithosphere is delaminated by convective instability and returns to the sublithospheric mantle (Eq. (20)).

(a hypothetical temperature of the mantle when it is adiabatically brought up to the surface without melting) and the vigor of convection, the latter of which is in turn affected by the consequences of mantle melting, i.e., the growth of insulating crust and depleted mantle lithosphere. The vigor of convection is also reflected in the magnitude of mantle heat flux  $F_m$ , which affects the thermal structure of the crust. The parameterization of these interrelations is detailed in the following sections.

When describing the dynamics of a chemically evolving mantle, we need to carefully distinguish between similar-sounding terms. In this study, lithosphere is used synonymously with top thermal boundary layer, and includes the crust and the shallow mantle (Fig. 1). This shallow mantle is called the mantle lithosphere (ML). The mantle can be divided into the mantle lithosphere and the sublithospheric mantle (SLM), based on differences in their physical natures; the former transports heat by conduction

whereas the latter by convection. The mantle can also be classified by differences in its chemical nature, and here the depleted mantle lithosphere (DML) refers to the residual mantle after melting. We call the rest of the (less depleted) mantle source mantle (SM). DML is always a part of ML, but not all of SM has to convect as SLM. In this study, the primitive mantle (PM) refers to the initial mantle at the beginning of the martian history.

## 2.2. Mantle melting

The martian mantle is generally considered to be more iron-rich than Earth's mantle, and in case of the olivine-dominated system, its Mg# (defined as molar Mg/(Fe + Mg) × 100) is estimated to be ~75 (e.g., Dreibus and Wänke, 1985), substantially lower than Earth's value of ~90 (e.g., McDonough and Sun, 1995; Lyubetskaya and Korenaga, 2007). The low Mg# of the martian mantle is known to depress the solidus by a few tens of degrees (Hirschmann, 2000) and enhance melt productivity (Bertka and Holloway, 1994). Despite these differences, we still employ the melting model suggested for Earth's mantle because the parameterization of melt production associated with convection is uncertain by a factor of ~2 as demonstrated in this section; that is, the uncertainties in the parameterization will overwhelm the effects of the details in the melting behavior. For the same reason, we use the simple melting model of Korenaga et al. (2002c) instead of that of McKenzie and Bickle (1988), which was used in the modeling of Hauck and Phillips (2002). The more complex parameterization of McKenzie and Bickle (1988) does not necessarily result in a better approximation because it assumes equilibrium melting as opposed to more realistic fractional melting. Fractional melting in the upwelling mantle is a process complicated by the differential movements of melt and solid phases and by resulting chemical reactions at various depths, but its gross outcome may be captured reasonably well by adjusting a single parameter,  $(d\phi/dP)_s$ , which is the change in melt fraction caused by a change in pressure above the mantle solidus during adiabatic decompression (e.g., Kelemen and Holbrook, 1995).

Following Korenaga et al. (2002c), the initial pressure of melting,  $P_i$ , is related to the potential temperature as

$$P_i = \frac{T_u - 1423}{120 \times 10^{-9} - \left(\frac{dT}{dP}\right)_s}, \quad (3)$$

which is based on the solidus of dry peridotite (Takahashi and Kushiro, 1983). Here  $(dT/dP)_s$  is the adiabatic gradient in the mantle. Melting ceases when convective upwelling vanishes at the base of the top thermal boundary layer, so the final pressure of melting is given by

$$P_f = \rho_m g (h_{\text{crust}} + h_{\text{ML}}), \quad (4)$$

where  $g$  is gravitational acceleration,  $h_{\text{crust}}$  is crustal thickness, and  $h_{\text{ML}}$  is the thickness of the mantle lithosphere, which is the top thermal boundary layer within the mantle. This boundary layer thickness may be calculated by

$$h_{\text{ML}} = \frac{h_m}{Nu}, \quad (5)$$

where  $h_m$  is the thickness of the whole mantle and  $Nu$  is the Nusselt number for mantle convection. The Nusselt number is heat flux normalized by conductive heat flux and is calculated from the heat-flow scaling law for stagnant-lid convection (Section 2.4). If the initial pressure of melting is greater than the final, the mantle may be considered to be melting. The melt fraction is zero at the initial depth of melting and linearly increases to the maximum at the base of the thermal lithosphere, so the average melt fraction in the melting zone is given by

$$\phi = \frac{P_i - P_f}{2} \left(\frac{d\phi}{dP}\right)_s. \quad (6)$$

To calculate the volumetric melt production, we assume the upwelling mantle is approximately cylindrical and calculate the flux of material through the depth range bounded by the initial and final pressures of melting (Reese et al., 1998). We take the radius of the cylinder to be equal to the mantle depth,  $h_m$ , because the aspect ratio of convection cells is typically ~1. In stagnant-lid convection, downwelling material tends to be much more focused than upwelling material (e.g., Solomatov and Moresi, 2000), so we may also assume that all downwelling occurs at the edge of the cylinder. The flux of mantle leaving the melting zone is  $2\pi h_m d_m u_i$ , where  $d_m$  is the height of the melting region and  $u_i$  is the convecting velocity of the mantle (Section 2.4). The total melt flux for the cylinder can be obtained by multiplying the average melt fraction, i.e.,  $2\pi h_m d_m u_i \phi$ , so the melt productivity per unit area is given by  $2d_m u_i \phi / h_m$ . The whole-planet melt productivity may thus be parameterized as

$$f_m = \frac{2\gamma d_m u_i \phi}{h_m} \cdot 4\pi R_m^2. \quad (7)$$

The constant  $\gamma$  is 1 if we accept the above reasoning, but it can be as low as 0.5 if upwelling and downwelling are symmetrical and can also exceed 1 if the aspect ratio is smaller than 1. Such uncertainty is hard to eliminate in this type of order-of-magnitude derivation, but as shown later (Section 3.2), model results are not very sensitive to the exact value of  $\gamma$ .

## 2.3. Mass transport of incompatible elements

The source mantle becomes depleted in incompatible elements over time. Heat-producing elements and hydrogen are both incompatible and important to mantle dynamics. We therefore need to keep track of the volume of the mantle processed by melting in order to determine the changing concentrations of incompatible elements in the source mantle and in the crust.

Element partitioning by melting follows the following formula:

$$\frac{C_{\text{melt}}}{C_0} = \frac{1}{\phi + D(1 - \phi)}, \quad (8)$$

for equilibrium melting, and

$$\frac{C_{\text{melt}}}{C_0} = \frac{1}{\phi} \left[ 1 - (1 - \phi)^{1/D} \right], \quad (9)$$

for accumulated fractional melting, where  $C_0$  is the initial concentration in the solid before melting,  $C_{\text{melt}}$  is the concentration in the melt, and  $D$  is the bulk distribution coefficient (Shaw, 1970). Incompatible elements have  $D$  lower than 1. The  $D$  value for hydrogen is ~0.002 in olivine/basalt (Koga et al., 2003) and ~0.02 in pyroxene/basalt (Hirschmann et al., 2005). Assuming that olivine and pyroxenes occupy the 60% and 40% of the mantle, respectively (i.e., Earth-like mantle), therefore, the bulk distribution coefficient for hydrogen is ~0.01. Here pyroxenes include both clinopyroxene and orthopyroxene. The  $D$  values for heat-producing elements (U, Th, and K) are ~0.01 in clinopyroxene/basalt (Hart and Dunn, 1993; Hauri et al., 1994) and vanishingly small in other systems (e.g., Beattie, 1993), so given that clinopyroxene occupies ~20% of Earth's upper mantle, the bulk distribution coefficients for heat-producing elements can be as low as ~0.002. With accumulated fractional melting, which is more appropriate for mantle melting than equilibrium melting, >90% dehydration is expected for  $\phi > 0.02$  and a nearly complete extraction of heat-producing elements for  $\phi > 0.01$  (Fig. 2).

To facilitate the modeling of mass transport, we assume  $D = 0$  and also consider mantle melting only when the melt fraction

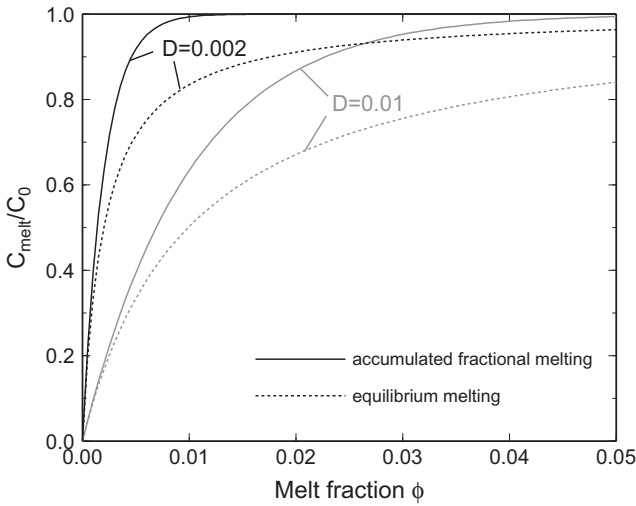


**Fig. 2.** Extraction of incompatible elements by equilibrium melting (dashed) and accumulated fractional melting (solid). The ratio  $C_{\text{melt}}/C_0$  is shown as a function of melt fraction  $\phi$  in the cases of  $D = 0.01$  (gray) for the partitioning of hydrogen and  $D = 0.002$  (black) for that of heat-producing elements.

calculated from Eq. (6) exceeds some threshold (e.g., 0.01). That is, when  $\phi$  happens to be smaller than the threshold at some time step, we do not extract melt (thus incompatible elements as well) from the source mantle and proceed to the next time step. We find that the model behavior is virtually insensitive to this critical melt fraction. We may use 0.02 instead of 0.01, for example, and still obtain essentially the same results. This is because when mantle is melting in the early Mars, melt fraction higher than the critical is usually achieved so the system behaves as if  $D = 0$ , as long as the critical melt fraction is not too large (e.g.,  $>0.05$ ).

The chemical evolution of the source mantle is tracked through the following five volumes: the volume of the initial primitive mantle (PM),  $V_{\text{PM}}$ , the volume of the source mantle,  $V_{\text{SM}}(t)$ , the volume of the depleted mantle lithosphere,  $V_{\text{DML}}(t)$ , the volume of the processed mantle,  $V_{\text{processed}}(t)$ , and the crustal volume,  $V_{\text{crust}}(t)$ . We neglect small density difference between different volumes, so the following relation always holds:

$$V_{\text{SM}}(t) + V_{\text{DML}}(t) + V_{\text{crust}}(t) = V_{\text{PM}}. \quad (10)$$

Assuming that all melt is extracted to form crust, an increase in the crustal volume at a given time interval  $\Delta t$  is given by

$$\Delta V_{\text{crust}}(t) = f_m(t) \Delta t, \quad (11)$$

and a change in the DML volume is

$$\Delta V_{\text{DML}}(t) = f_m(t) \frac{(1 - \phi)}{\phi} \Delta t. \quad (12)$$

The amount of mantle that has been melted during the interval is equal to

$$\Delta V_{\text{processed}}(t) = -\Delta V_{\text{SM}}(t) = \frac{f_m(t)}{\phi} \Delta t. \quad (13)$$

As described later, the DML volume can decrease if a fraction of DML delaminates by convective instability, but the volume of the processed mantle monotonically increases and could potentially exceed  $V_{\text{PM}}$ , which means that the entire mantle has been melted at least once. The crustal thickness is calculated from the crustal volume based on the following geometrical relation:

$$V_{\text{crust}}(t) = \frac{4\pi}{3} \left\{ R_p^3 - (R_p - h_{\text{crust}}(t))^3 \right\}, \quad (14)$$

and the DML thickness is calculated in a similar manner.

The amount of heat that would be produced in the undifferentiated primitive mantle may be expressed as

$$H_{\text{PM}}(t) = V_{\text{PM}} Q_0 e^{-\lambda t}, \quad (15)$$

where  $Q_0$  is the initial heat source density and  $\lambda$  is the decay constant. Here we are approximating the decay of different radiogenic isotopes collectively by one ‘effective’ decay (Stevenson et al., 1983). The crustal heat production may be tracked as

$$H_{\text{crust}}(t) = H_{\text{crust}}(t - \Delta t) e^{-\lambda \Delta t} + Q_{\text{SM}}(t) \Delta V_{\text{processed}}(t), \quad (16)$$

where  $Q_{\text{SM}}(t)$  is the volumetric heat production of the source mantle calculated as

$$Q_{\text{SM}}(t) = \frac{H_{\text{PM}}(t) - H_{\text{crust}}(t)}{V_{\text{SM}}(t)}. \quad (17)$$

The whole-mantle heat production  $Q_m$  needed for Eq. (1) can be prepared by multiplying  $V_{\text{SM}}/(V_{\text{SM}} + V_{\text{DML}})$  and the above.

The dehydration of the mantle is tracked in a similar manner, but in this case we assume that all water extracted by melting is brought to the planet’s surface:

$$V_{\text{surface}}^W(t) = V_{\text{surface}}^W(t - \Delta t) + C_{\text{SM}}^W(t) \Delta V_{\text{processed}}(t), \quad (18)$$

where  $V_{\text{surface}}^W(t)$  represents the total volume of water brought to the surface by time  $t$  and  $C_{\text{SM}}^W$  is the concentration of water in the source mantle. We choose to normalize the water concentration by the initial concentration, so the unit of the water volume is arbitrary. The water concentration in SM can be calculated as

$$C_{\text{SM}}^W(t) = \frac{V_{\text{SM}}^W(t)}{V_{\text{SM}}(t)} = \frac{V_{\text{PM}}^W - V_{\text{surface}}^W(t)}{V_{\text{SM}}(t)}. \quad (19)$$

There are two further processes that need to be modeled regarding chemical evolution. The first one is lithospheric delamination. As mentioned in Section 2.2, the thickness of the top thermal boundary layer in the mantle is calculated from the heat-flow scaling of stagnant-lid convection (Eq. (5)). If we encounter the situation in which  $h_{\text{DML}} > h_{\text{ML}}$ , this means that DML is not strong enough or not buoyant enough to remain intact and that a part of DML outside the boundary layer should be destabilized and recycled back to the source mantle. When this happens, therefore, we denote the excess DML thickness as  $\Delta_1 h_{\text{DML}} (= h_{\text{DML}}(t^-) - h_{\text{ML}}(t))$  and update the DML thickness as

$$h_{\text{DML}}(t^+) = h_{\text{ML}}(t), \quad (20)$$

where  $t^-$  and  $t^+$  denote time infinitesimally earlier and later than  $t$ , respectively. The volumes of DML and SM are adjusted accordingly. The heat production and water concentration of SM are both affected by this delamination, so they must be updated by multiplying the factor  $V_{\text{SM}}(t^+)/V_{\text{SM}}(t^-)$ . Here we are assuming that the delaminated lithosphere is efficiently mixed with the convecting mantle.

The second process is the re-hydration of DML from below by hydrogen diffusion (Korenaga, 2009b). The dehydrated mantle is always underlain by the more hydrated source mantle, so it is continuously subjected to rewetting from below. Based on numerical modeling, Korenaga (2009b) derived the following approximate formula for the diffusion distance of hydrogen under lithospheric conditions:

$$\Delta_2 h_{\text{DML}} \approx (D_{\text{H,eff}}^* D_{\text{H},0} t_{\text{diff}})^{1/2}, \quad (21)$$

where  $D_{\text{H},0} = 6 \times 10^{-5} \text{ m}^2 \text{ s}^{-1}$  and

$$D_{\text{H,eff}}^* = -0.0027 + 2.19 \times 10^{-6} (\bar{T}_u - 273). \quad (22)$$

The diffusion time  $t_{\text{diff}}$  is time duration relevant for this diffusion process, and  $\bar{T}_u$  is the upper mantle temperature averaged over this duration. When lithospheric delamination takes place,

for example, the diffusion time may be reset to zero if  $\Delta_1 h_{\text{DML}} > \Delta_2 h_{\text{DML}}$  (i.e., all of the rewetted region is delaminated).

Because the mantle lithosphere can delaminate, the SM composition is not guaranteed to stay at the initial PM composition. Though delamination can affect the SM composition considerably in terms of minor incompatible elements such as hydrogen and heat-producing elements, it does not substantially modify its major element composition, i.e., the fertility of SM. Therefore the use of Eq. (3) should be approximately valid even with the varying SM composition.

#### 2.4. Mantle rheology and the scaling of stagnant-lid convection

We assume the following Newtonian rheology when considering the scaling of stagnant-lid convection:

$$\mu(T_u, C_{\text{SM}}^W) = A \exp \left[ \frac{E}{RT_u} + (1 - C_{\text{SM}}^W) \log \Delta\mu \right], \quad (23)$$

where  $A$  is the preexponential factor,  $E$  is the activation energy,  $R$  is the universal gas constant, and  $\Delta\mu$  is the viscosity contrast between wet and dry mantle. As mentioned earlier,  $C_{\text{SM}}^W$  is a normalized concentration so that it has an initial value of one and decreases toward zero as the mantle dehydrates.

The rheology of silicate minerals is known to be generally more complex than the above Newtonian rheology. The olivine-dominated system, for example, can deform by both diffusion (Newtonian) and dislocation (non-Newtonian) creep mechanisms under typical mantle conditions (Karato and Wu, 1993; Hirth and Kohlstedt, 2003). The existing scaling laws of stagnant-lid convection can handle each type of rheology independently (e.g., Solomatov and Moresi, 2000) but not the combination of them (known as ‘composite’ rheology). At the same time, nontrivial experimental uncertainty still exists even for the rheology of olivine aggregates (Korenaga and Karato, 2008), and it is difficult to consider the full complexity of mantle rheology and treat its uncertainty in a proper manner. Our intention behind Eq. (23) is to formulate temperature- and composition-dependent rheology with the least number of parameters ( $A$ ,  $E$ , and  $\Delta\mu$ ) so that model sensitivity to them can easily be explored. Non-Newtonian rheology may be approximated by Newtonian rheology using the ‘effective’ activation energy (Christensen, 1984), and  $E$  of  $\sim 300 \text{ kJ mol}^{-1}$  corresponds to both diffusion and dislocation creep under this approximation (Korenaga, 2006). The constant  $A$  is determined by prescribing the reference viscosity  $\mu_0$  at the reference temperature  $T_{u,0}$  and at  $C_{\text{SM}}^W = 1$ , and we will test a range of  $\mu_0$  and  $\Delta\mu$  to cover the uncertainty of mantle rheology.

Thermal convection with purely temperature-dependent viscosity can be characterized by two nondimensional parameters, the internal Rayleigh number  $Ra_i$  and the Frank–Kamenetskii parameter  $\theta$  (Solomatov, 1995). The internal Rayleigh number is a measure of potential convective vigor and is defined here as

$$Ra_i = \frac{\alpha_m \rho_m g (T'_u - T_{\text{crust}}) h_m^3}{\kappa_m \mu(T_u, C_{\text{SM}}^W)}, \quad (24)$$

where  $\alpha_m$  and  $\kappa_m$  are the thermal expansivity and thermal diffusivity of the mantle, respectively,  $T'_u$  is the mantle potential temperature at the top of the mantle, and  $T_{\text{crust}}$  is the temperature at the base of the crust (Fig. 1).  $T'_u$  is similar to  $T_u$  but measured at the top of the mantle instead of the surface (Fig. 1). These two potential temperatures are not very different when crustal thickness is on the order of only 100 km, but to be precise, the difference between  $T'_u$  and  $T_{\text{crust}}$  is the temperature scale relevant for stagnant-lid convection beneath the crust. The Frank–Kamenetskii parameter is related to the temperature dependency of viscosity as

$$\theta = \frac{E(T'_u - T_{\text{crust}})}{RT_u^2}. \quad (25)$$

When the activation energy is on the order of a few hundreds  $\text{kJ mol}^{-1}$ ,  $\theta$  usually takes a value of  $\sim 20$ , which is sufficiently large to bring the convection system to the stagnant-lid regime (Solomatov, 1995).

For stagnant-lid convection with purely temperature-dependent viscosity, the scaling law of average convective velocity beneath the lid may be expressed as (Solomatov and Moresi, 2000):

$$u_i = 0.38 \frac{\kappa_m}{h_m} \left( \frac{Ra_i}{\theta} \right)^{1/2}, \quad (26)$$

and the Nusselt number is given by

$$Nu = 0.53 \theta^{-4/3} Ra_i^{1/3}. \quad (27)$$

Korenaga (2009b) showed that the velocity scaling of (26) is still approximately valid even with the effects of compositional buoyancy and dehydration stiffening, but the scaling of the Nusselt number (i.e., normalized heat flux) is substantially modified. A closed-form formula such as Eq. (27) is not available in this case, and the Nusselt number needs to be calculated based on the local stability analysis at each time step, the functionality of which may be symbolically expressed as

$$Nu = F_{\text{Nu}}(Ra_i, E, T_u, T_{\text{crust}}, h_{\text{DML}}/h_m, \Delta_2 h_{\text{DML}}/h_m, \Delta\mu^{C_{\text{SM}}^W}, \Delta\rho), \quad (28)$$

where  $\Delta\mu^{C_{\text{SM}}^W}$  and  $\Delta\rho$  are, respectively, the viscosity and density contrasts between SM and DML. Rewetting of DML from below (Section 2.3) affects the dehydrated nature of DML but not its chemical buoyancy, and the use of  $\Delta_2 h_{\text{DML}}/h_m$  in the above signifies that we distinguish between the thickness of buoyant lithosphere and that of dehydrated lithosphere in the stability analysis. The density contrast is calculated from the average degree of melting for the entire DML as (Korenaga, 2009b):

$$\Delta\rho = 1 + \frac{\bar{\phi}}{\rho_m} \left( \frac{d\rho}{d\phi} \right). \quad (29)$$

The effect of mantle melting on lithospheric density may be quantified as

$$\frac{d\rho}{d\phi} = \frac{d\rho}{d\text{Mg}\#} \frac{d\text{Mg}\#}{d\phi}, \quad (30)$$

where  $\text{Mg}\#$  is defined as  $100 \times$  molar  $\text{Mg}/(\text{Mg} + \text{Fe})$  of mantle composition. The extensive compilation of mantle xenolith data suggests that  $(d\rho/d\text{Mg}\#)$  is likely to be  $-15 \text{ kg m}^{-3} \text{ Mg}\#^{-1}$  (Lee, 2004). Mantle melting models generally show that  $\text{Mg}\#$  increases  $\sim 0.08\%$  of melt removal (e.g., Kinzler and Grove, 1992; Langmuir et al., 1992), i.e.,  $(d\text{Mg}\#/d\phi) \sim 8 \text{ Mg}\#$ . We therefore set  $(d\rho/d\phi)$  to  $-120 \text{ kg m}^{-3}$  when testing the effect of compositional buoyancy.

Note that even in the scaling law of Eq. (28) the distribution of heat production in the mantle is still assumed to be homogeneous, which is apparently inconsistent with the notion of chemically depleted lithosphere. The thermal effect of depleted lithosphere, however, can be shown to be negligibly small as follows. The non-dimensionalized thickness of mantle lithosphere may be expressed as

$$\frac{h_{\text{ML}}}{h_m} = 1 - \left[ 1 - 2Nu^{-1} (1 - a_{rh} \theta^{-1}) \right]^{1/2} \quad (31)$$

for the homogeneous distribution of heat production, where  $a_{rh}$  is  $\sim 2.4$  for Newtonian rheology (see Appendix A of Solomatov and Moresi (2000) for materials necessary to derive this;  $h_{\text{ML}}/h_m$  here is equivalent to their  $\delta_L$ ). We can repeat the same exercise, but with all heat production being concentrated in the sublithospheric mantle, to arrive at

$$\frac{h_{ML}}{h_m} = Nu^{-1}(1 - a_{rh}\theta^{-1}). \quad (32)$$

For plausible parameter range expected for  $\theta$  and  $Nu$ , the difference between Eqs. (31) and (32) is only a few percent, which is substantially smaller than a factor of 5–10 difference caused by dehydration stiffening and chemical buoyancy (Korenaga, 2009b).

### 2.5. Surface, mantle, and core heat flows

As seen in the previous section, the temperature difference driving mantle convection is  $T'_u - T_{crust}$ , and the temperature at the base of the crust (i.e., the Moho temperature) needs to be determined self-consistently with mantle heat flux and heat production within the crust. The crustal thermal structure can be of critical importance for mantle dynamics; if the Moho temperature approaches the upper mantle temperature, for example,  $Ra_i$  becomes vanishingly small and convection ceases. We solve this problem by a finite-difference scheme as describe below.

Suppose that the crustal thickness increases by  $\Delta h_{crust}$  at time  $t$ . We then construct a new thermal profile across the crust as

$$T(t^+, z) = \frac{1}{h_{crust}(t)} \{T(t - \Delta t, \beta z)h_{crust}(t - \Delta t) + T_u(t)\Delta h_{crust}\}, \quad 0 \leq z \leq h_{crust}(t), \quad (33)$$

where  $\beta = h_{crust}(t)/h_{crust}(t - \Delta t)$ . That is, we extend the original thermal profile to fit the new crustal thickness and mix in hot new crustal material uniformly. This might correspond to the case of crustal growth by pervasive melt percolation. Actual crustal growth would proceed by episodic and localized eruptions and intrusions, but our simple strategy may be sufficient to appreciate the thermal impact of new crustal addition on the spherically averaged thermal structure. Using this new profile at  $t^+$  as the initial condition, we solve the following heat conduction equation for the next time step  $t + \Delta t$ :

$$\rho_{crust}c_{crust}\frac{\partial T}{\partial t} = \frac{\partial}{\partial z} \left( k_{crust} \frac{\partial T}{\partial z} \right) + Q_{crust}(z), \quad (34)$$

with the boundary conditions of  $T(z=0) = T_s$  and

$$k_{crust} \left. \frac{\partial T}{\partial z} \right|_{z=h_{crust}} = F_m(t - \Delta t). \quad (35)$$

Here  $\rho_{crust}$ ,  $c_{crust}$ , and  $k_{crust}$  are the density, specific heat, and thermal conductivity of the crust, respectively. To be consistent with our treatment of crustal volume (Section 2.3), however, these crustal variables are assumed to take mantle values.

Though the above equation does not take into account the latent heat of crystallization explicitly, a comparable effect is expected to be achieved by the direct use of mantle potential temperature  $T_u$  in Eq. (33) because the actual melt temperature should be lower than  $T_u$  by a few hundreds K owing to the extraction of the latent heat of fusion (e.g., McKenzie and Bickle, 1988; Langmuir et al., 1992). The volumetric heat production of the crust,  $Q_{crust}(z)$ , is calculated from the total crustal heat production  $H_{crust}$  assuming an exponential distribution with the  $e$ -folding length scale of  $h_r$ . The mantle heat flux is taken from the previous time step, and error caused by this approximation should diminish as  $\Delta t \rightarrow 0$ . We use the backward Euler method, which is unconditionally stable, to solve the discretized version of the above equation in one step, and the new Moho temperature at  $t + \Delta t$  is taken from the updated profile. The surface heat flux,  $F_s$ , is calculated from the crustal thermal profile as

$$F_s = k_{crust} \left. \frac{\partial T}{\partial z} \right|_{z=0}. \quad (36)$$

Once the Moho temperature is determined, it is straightforward to calculate the mantle heat flux:

$$F_m = k_m \frac{Nu(T'_u - T_{crust})}{h_m}, \quad (37)$$

where  $k_m$  is the thermal conductivity of the mantle. It takes finite time for mantle heat flux to adjust to a given boundary condition, but as shown later, the Moho temperature varies most considerably at the beginning of the martian history when the mantle is still hot and thus has low viscosity. In this case, the adjustment time scale is expected to be on the order of 10 Myr (Korenaga, 2009a), so our treatment should not be grossly in error. Note that our way of thermally separating the mantle and the crust and using a matching condition between the two is internally consistent, but one can still question how accurately it could capture the gross planetary evolution. In this sense, our attempt should be regarded as one reasonable attempt but not the only one. In particular, the thermal evolution of growing crust may be better parameterized after modeling coupled crust–mantle evolution in 2-D or 3-D.

For the core heat flux, we adopted the method of Stevenson et al. (1983) with no modification. In particular, we use the same mantle rheology assumed by them (purely temperature-dependent viscosity), which is different from Eq. (23), when evaluating the stability of the thermal boundary layer above the core. There are two reasons for this strategy. First, the core–mantle boundary (CMB) region of Mars is likely to have a mineralogical composition similar to that of Earth's lower mantle (e.g., Bertka and Fei, 1998), so the rheology relevant to the CMB dynamics is different from what we need for the scaling of stagnant-lid convection, which is primarily controlled by upper mantle rheology. Second, we would like to focus on how thermal evolution is affected by mantle melting, and leaving other parts of the model untouched makes it easier to understand the significance of melting effects. The rheology of the martian lower mantle does not have to be similar to what is assumed by Stevenson et al. (1983), but our current understanding of lower mantle rheology is still highly limited. We also set the mass fraction of light elements in the core to be 0.2, to avoid the solidification of the inner core throughout the entire history of Mars (Schubert et al., 1992); once the solid inner core starts to form, it is virtually impossible to shut down the martian dynamo, thereby becoming inconsistent with the absence of the martian magnetic field at the present day.

### 3. Results

We calculated the thermal history of Mars following the theoretical formulation described above, with no crustal layer at the beginning, for the duration of 4.5 byr. The numerical integration was done with the forward Euler method using a time step of 1 myr, which was found to be sufficient (less than 1% error) by testing with smaller time steps. Important 'free' parameters in our formulation include: the initial mantle temperature  $T_u(0)$ , the initial core temperature  $T_{cm}(0)$ , the initial heat production in the mantle  $Q_0$ , the viscosity contrast between wet and dry mantle  $\Delta\mu$ , the degree of compositional buoyancy ( $d\rho/d\phi$ ), the scaling factor in the melt productivity formula  $\gamma$ , the depth distribution of heat production with the crust as specified by the  $e$ -folding length scale  $h_r$ , the reference mantle viscosity  $\mu_0$ , and the activation energy  $E$  for temperature-dependent mantle rheology. For some parameters, we found that modeling results were not very sensitive to variations within their plausible range, which helped us to focus on examining the effects of varying a subset of these nine free parameters. In this section, we will first show a few representative model results and explain them in some detail. Results from exploratory sensitivity tests are also discussed. We surveyed the parameter space extensively, by testing all possible combinations of variations in important free parameters, and results from these permutation runs are summarized at the end.

### 3.1. Thermal evolution with and without dehydration stiffening and compositional buoyancy

To facilitate comparison with previous studies, some parameter values used in this section are taken from the ‘nominal’ model of Hauck and Phillips (2002):  $T_u(0)$  and  $T_{cm}(0)$  are arbitrarily assigned values of 1750 K and 2000 K, respectively. The amount of internal heat production  $Q_0$  is set to  $8.25 \times 10^{-8} \text{ W m}^{-3}$ , which corresponds to the chondritic composition model of Mars (Wänke and Dreibus, 1994). The reference mantle viscosity is set to  $10^{19} \text{ Pa s}$  at  $T_{u,0}$  of 1573 K, based on estimated viscosity for Earth’s (moderately wet) suboceanic mantle at the present day (Hager, 1991; Hirth and Kohlstedt, 1996). The activation energy is fixed here to  $300 \text{ kJ mol}^{-1}$  (Korenaga, 2006), and we further set  $\gamma$  and  $h_r/h_{crust}$  to be 1 and 1/4, respectively.

Modeling results are shown in Fig. 3 for five cases with different combinations of  $\Delta\mu$  and  $(d\rho/d\phi)$ . One of them has  $\Delta\mu$  of 1 and  $(d\rho/d\phi)$  of 0, corresponding to the absence of both dehydration stiffening and compositional buoyancy (shown with solid curves in Fig. 3). In this case, the Moho temperature quickly increases to  $\sim 1450 \text{ K}$  in

the first 200 Myr (Fig. 3a), which is primarily caused by rapid crustal growth ( $>100 \text{ km}$  in thickness), and then slowly decreases (Fig. 3c). The mantle and core temperatures decrease monotonically, along with heat fluxes from the surface, the mantle, and the core (Fig. 3b). The positive correlation between the Moho temperature and the crustal thickness seen in the first 200 Myr may easily be understood from the following steady-state formula for the Moho temperature (e.g., Turcotte and Schubert, 1982, chap. 4):

$$T_{crust} = T_s + \frac{F_m}{k_{crust}} h_{crust} + \frac{Q_{crust}}{2k_{crust}} h_{crust}^2, \quad (38)$$

where a uniform distribution of internal heat production is assumed for simplicity. The mantle heat flux  $F_m$  is always positive (Fig. 3b), and radiogenic elements are efficiently transported into the crust by mantle melting (Fig. 3e), so the Moho temperature is expected to increase nonlinearly when the crust thickens. Though the above formula is derived for a steady state (i.e.,  $\partial T/\partial t = 0$ ), we found that it is still a good approximation to our finite-difference solutions. The subsequent gradual decrease in the Moho temperature reflects the radiogenic decay of heat-producing elements in the crust.

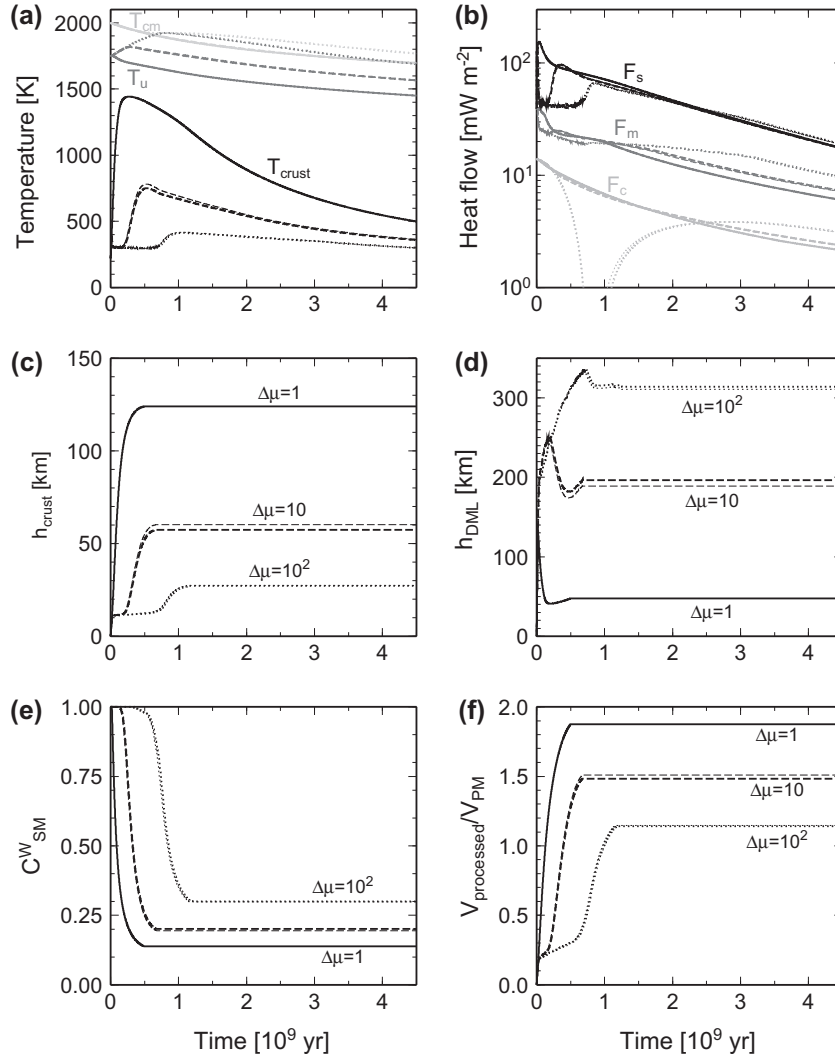


**Fig. 3.** Representative models showing thermal evolution and crustal growth. Solid curves show the reference case without these effects ( $\Delta\mu$  of 1 and  $(d\rho/d\phi)$  of 0). Dashed and dotted curves correspond to  $\Delta\mu$  of 10 and 100, respectively; thinner ones are for the cases with compositional buoyancy ( $(d\rho/d\phi)$  of  $-120 \text{ kg m}^{-3}$ ). In all cases, the initial mantle temperature  $T_u(0)$  is 1750 K, the initial core temperature  $T_{cm}(0)$  is 2000 K,  $\gamma$  is 1, the reference viscosity  $\mu_0$  is  $10^{19} \text{ Pa s}$ , the activation energy  $E$  is  $300 \text{ kJ mol}^{-1}$ ,  $h_r/h_{crust}$  is 1/4, and the initial internal heat production  $Q_0$  is  $8.25 \times 10^{-8} \text{ W m}^{-3}$ . (a) Moho temperature (black), mantle temperature (dark gray), and core temperature (light gray). (b) Surface heat flux (black), mantle heat flux (dark gray), and core heat flux (light gray). (c) Crustal thickness. (d) Thickness of depleted mantle lithosphere. (e) Normalized water concentration in the source mantle. (f) Volume of processed mantle normalized by that of entire mantle. All shown as a function of time in billion years.

The evolution of DML and the processed mantle (Fig. 3d and f) is worth noting. As mantle melting proceeds, DML quickly thickens to  $\sim 130$  km (within the first 20 Myr), but then erodes down to  $\sim 50$  km by convective instability, which is enhanced by the increased Moho temperature. Lithospheric delamination helps the underlying source mantle to rise and melt more, resulting in the almost two-time processing of the entire mantle (Fig. 3f). Because delamination also dilutes the concentration of trace elements in the source mantle, however, the source mantle is not completely depleted even after such efficient processing (Fig. 3e).

Four other cases shown in Fig. 3 are models with dehydration stiffening ( $\Delta\mu = 10$  and 100) with and without compositional buoyancy ( $(d\rho/d\phi) = 0$  and  $-120 \text{ kg m}^{-3}$ ). Dehydration stiffening tends to stabilize the DML (Fig. 3d), which then limits melt production, crustal growth, and mantle processing (Fig. 3c and f). The Moho temperature is suppressed as well as the cooling of the mantle (Fig. 3a). With  $\Delta\mu$  of 10, for example, the crust stops growing at  $\sim 60$  km, and the maximum temperature achieved within the crust is less than 800 K ( $\sim 550$  °C). When  $\Delta\mu$  is as high as 100, the mantle is heated up by  $\sim 150$  K during the first 0.8 Gyr, and the core stops its cooling temporarily at  $\sim 0.7$ – $1.1$  Gyr (Fig. 3b). Interestingly, the cases with compositional buoyancy are barely distinguishable from those without one. This is surprising because the preliminary scaling suggests that compositional buoyancy in the presence of dehydration stiffening helps to stabilize DML when the mantle temperature exceeds  $\sim 1800$  K (Fig. 13a, Korenaga, 2009b). The reason for this apparent insignificance of compositional buoyancy is the following. Compositional buoyancy helps to suppress convective instability and generate thicker DML, but then the thickened DML insulates the mantle better and the resulting higher mantle temperature facilitates the convective delamination of the bottom fraction of DML. This negative feedback, which has already been recognized by Parmentier and Hess (1992) in the oscillatory behavior of DML dynamics, may be important when understanding lithospheric dynamics at regional scales but does not affect the long-term evolution. Hereinafter, we will always include compositional buoyancy with  $(d\rho/d\phi)$  of  $-120 \text{ kg m}^{-3}$  whenever dehydration stiffening is considered (i.e.,  $\Delta\mu > 1$ ) to consider the full effects of mantle melting, but dehydration stiffening is always considerably more important than compositional buoyancy.

### 3.2. Model sensitivity to some key parameters

In this section, we use the case with  $\Delta\mu$  of 10 and  $(d\rho/d\phi)$  of  $-120 \text{ kg m}^{-3}$  from the previous section as a reference (shown as solid curves), against which several sensitivity tests are conducted. This case predicts  $\sim 60$ -km-thick crust, which is intermediate among existing estimates on martian crustal thickness (30–115 km) (Zuber et al., 2000; Zuber, 2001; Nimmo and Stevenson, 2001; McGovern et al., 2002; Wiczcerek and Zuber, 2004). When we vary the value of a particular parameter explained in the following section, other parameters are always fixed to their values in the reference model.

As mentioned in Section 2.2, the parameterization of melt productivity (Eq. (7)) is uncertain at least by a factor of 2. We first varied the scaling factor  $\gamma$  in Eq. (7) from 0.5 to 2, but found that the results from these cases are not very different from the reference case with  $\gamma = 1$  (Fig. 4a, d, and g). This lack of sensitivity to as much as 4-fold increase in melt productivity suggests that convective velocity is always fast enough to convert all source mantle above the initial depth of melting to depleted mantle. Larger  $\gamma$  simply reaches this saturated state faster and does not necessarily result in thicker crust. As the mantle cools down, convection velocity decreases, so there may be a period during which a difference in  $\gamma$  may matter. Such a period, however, would not last long because

the mantle eventually becomes too cold to melt and how the melt productivity is parameterized is no longer relevant.

Next, we tested different depth distributions of crustal heat production. The reference case assumes a value for  $h_r/h_{\text{crust}}$  of 1/4, so heat production is more concentrated in the top quarter of the crust. The notion of the exponential distribution of heat production originates in the study of Earth's continental crust (Lachenbruch, 1970), but in recent years it has been suggested that the actual distribution may not take such exponential form (e.g., Jaupart and Mareschal, 2003). The martian crust, however, is probably closer to Earth's oceanic crust in terms of chemical composition, which implies that primary melt for the crust was produced by single-stage mantle melting and also experienced crystal fractionation during its ascent to the surface. In this case, the exponential distribution would be a good approximation because the lower crust, which may be dominated by fractionated cumulates, is expected to be depleted in heat-producing elements. Nonetheless, the depth distribution of heat production in the martian crust is not constrained by observations, so we tested two additional values, 1/2 and  $\infty$ , for  $h_r/h_{\text{crust}}$  (Fig. 4a, d, and g). The latter corresponds to a uniform distribution. Different depth distributions result in considerably different evolution scenarios, with more uniform distribution yielding higher Moho temperature, thicker crust, and thinner DML. These correlations among the Moho temperature, crustal thickness, and DML thickness is similar to what is achieved by varying the viscosity contrast  $\Delta\mu$  (Fig. 3).

In our formulation, the rheology of the mantle is controlled by the reference viscosity, the activation energy, and the viscosity contrast between dry and wet mantle (Eq. (23)). The effect of varying the last parameter was discussed in the previous section, so we test the model sensitivity to the other two. We first varied the activation energy  $E$  from 200 to 400  $\text{kJ mol}^{-1}$ ; if interpreted as the effective activation energy, this range is sufficiently wide to cover the likely uncertainty of olivine rheology (Korenaga and Karato, 2008). Lower activation energy leads to more vigorous convection and produces thicker crust, but differences caused by varying  $E$  is rather small (Fig. 4b, e, and h). In contrast, varying the reference viscosity (at the temperature of  $T_{u,0} = 1573$  K) by one order of magnitude results in a drastic change in the model behavior. Existing estimates for the viscosity of Earth's suboceanic mantle are characterized by this degree of uncertainty (e.g., Hager, 1991; Davaille and Jaupart, 1994; Watts and Zhong, 2000; Korenaga and Jordan, 2002a), so the high model sensitivity to the (poorly constrained) reference viscosity should always be kept in mind when discussing thermal evolution.

Lastly, we varied the initial heat production  $Q_0$  and tested  $1.25 \times 10^{-7} \text{ W m}^{-3}$  and  $1.74 \times 10^{-7} \text{ W m}^{-3}$ . As mentioned previously, the reference value of  $8.25 \times 10^{-8} \text{ W m}^{-3}$  corresponds to the composition model of Wänke and Dreibus (1994) for the bulk silicate portion of Mars, with 305 ppm K, 56 ppb Th, and 16 ppb U. The relative abundance of the heat-producing elements is nearly chondritic in this model. A more K-rich composition has been proposed by Lodders and Fegley (1997) (920 ppm K, 55 ppb Th, and 16 ppb U) on the basis of the oxygen isotopic composition of the martian meteorites, and our highest  $Q_0$  corresponds to their model. As shown in Fig. 4f, this higher heat production results in too thick ( $\sim 200$  km) crust to be consistent with available observational constraints, so we decide not to explore the consequence of compositional uncertainty in order to keep our predictions of crustal thickness in a reasonable range.

### 3.3. Summary of permutation runs

Based on various sensitivity tests such as those reported in the previous section, we choose to investigate the behavior of thermal evolution models extensively, by varying all of the following

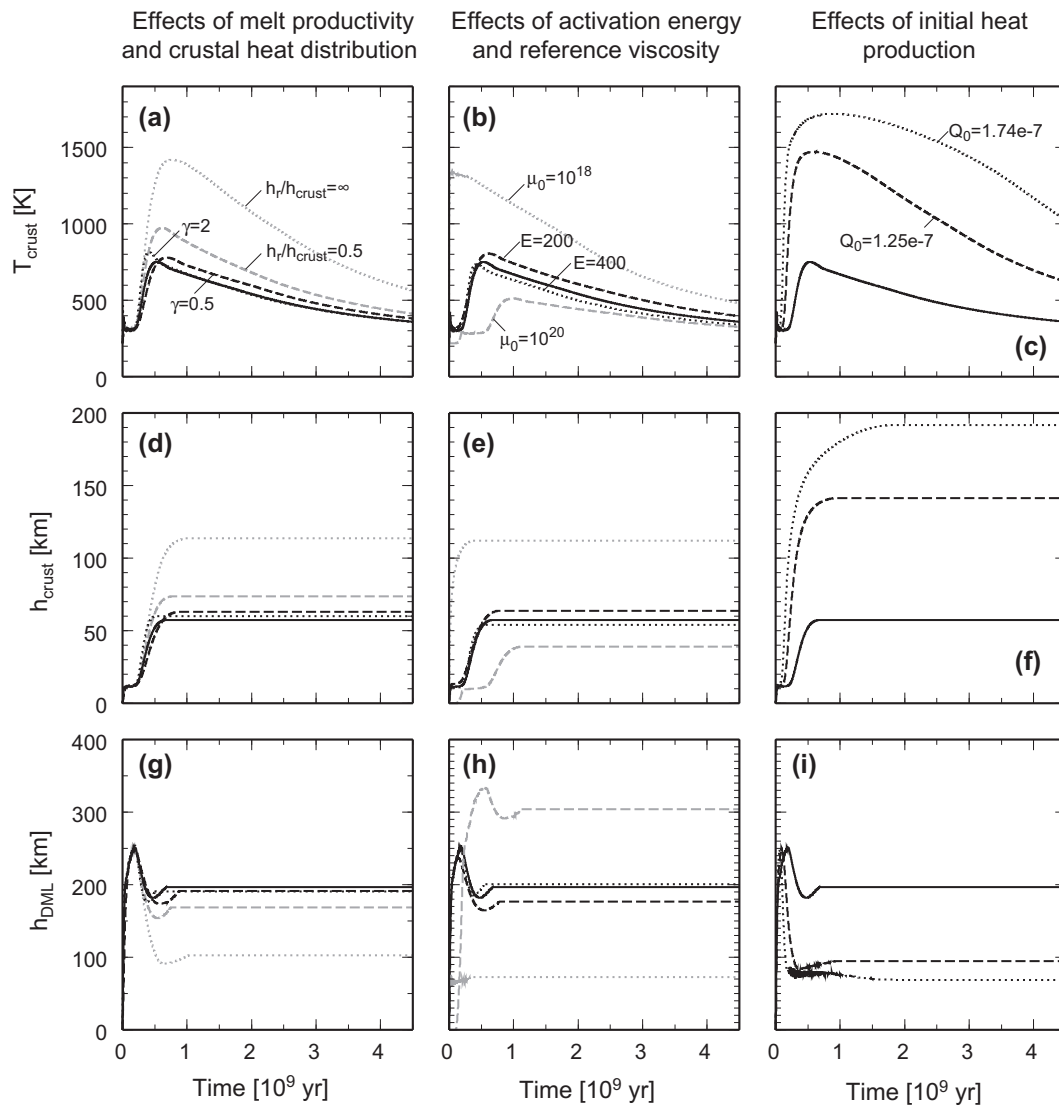


**Fig. 4.** Sensitivity tests to some key parameters. The reference model (shown by solid curves in all panels) is taken from Fig. 3 and has  $\Delta\mu$  of 10 and  $(d\rho/d\phi)$  of  $-120 \text{ kg m}^{-3}$ . (a–c) Moho temperature, (d–f) crustal thickness, and (g–i) DML thickness. Left: the effects of melt productivity (black dashed for  $\gamma = 0.5$  and black dotted for  $\gamma = 2$ ) and crustal heat production (gray dashed for  $h_r/h_{\text{crust}}$  of  $1/2$  and gray dotted for  $h_r/h_{\text{crust}}$  of  $\infty$ ). Middle: the effects of activation energy (black dashed for  $200 \text{ kJ mol}^{-1}$  and black dotted for  $400 \text{ kJ mol}^{-1}$ ) and reference viscosity (gray dashed for  $10^{20} \text{ Pa s}$  and gray dotted for  $10^{18} \text{ Pa s}$ ). Right: the effect of initial heat production (dashed for  $1.25 \times 10^{-7} \text{ W m}^{-3}$  and dotted for  $1.74 \times 10^{-7} \text{ W m}^{-3}$ ).

parameters: the initial mantle temperature  $T_u(0)$ , the initial core temperature  $T_{\text{cm}}(0)$ , the reference viscosity  $\mu_0$ , the viscosity contrast due to dehydration stiffening  $\Delta\mu$ , and the depth distribution of crustal heat production as characterized by  $h_r/h_{\text{crust}}$ . We test five values for  $T_u(0)$  (1550, 1650, 1750, 1850, 1950 K), three  $T_{\text{cm}}(0)$  (2000, 2100, 2200 K), three  $\mu_0$  ( $10^{18}$ ,  $10^{19}$ , and  $10^{20} \text{ Pa s}$ ), three  $\Delta\mu$  (1, 10, 100), and three  $h_r/h_{\text{crust}}$  (0.25, 0.5, and  $\infty$ ). Other parameters are set as:  $Q_0$  of  $8.25 \times 10^{-8} \text{ W m}^{-3}$ ,  $(d\rho/d\phi)$  of  $-120 \text{ kg m}^{-3}$ ,  $\gamma$  of 1, and  $E$  of  $300 \text{ kJ mol}^{-1}$ . We consider all permutations of the above values, i.e.,  $5 \times 3^4 = 405$  cases in total. The modeling results reveal interesting correlations among different variables, and we show them as a function of the present-day crustal thickness  $h_{\text{crust}}(t_p)$ , where  $t_p$  is 4.5 Gyr, in Figs. 5 and 6. As our primary objective is to identify the effect of dehydration stiffening on thermal evolution, we classify these correlations into two categories: one nearly independent of the degree of stiffening (Fig. 5) and the other strongly dependent of it (Fig. 6).

The observables in the first category include the water content in the present-day source mantle, the total volume of the pro-

cessed mantle, the maximum temperature experienced by the Moho, the present-day Moho temperature, and the present-day thickness of lithosphere. Plotting them as a function of  $h_{\text{crust}}(t_p)$  allows us to focus on the range relevant to the real Mars (i.e.,  $\sim 30$ – $115 \text{ km}$ ). For this range, the present-day source mantle is likely to have been dehydrated by more than  $\sim 80\%$  (Fig. 5a), and the entire mantle could have been processed at least once and maybe twice (Fig. 5b). Crustal thickness should be proportional to the degree of chemical differentiation experienced by the mantle, so these correlations are expected. The maximum crustal temperature during the martian history is below  $1500 \text{ K}$  for  $h_{\text{crust}}(t_p) < \sim 100 \text{ km}$ , and for the crustal thickness of  $50 \text{ km}$ , the maximum temperature is  $\sim 600$ – $800 \text{ K}$  (Fig. 5c). Also, dehydration stiffening tends to suppress the maximum Moho temperature. Such dependency on  $\Delta\mu$  is not observed for the present-day Moho temperature, the trend of which is defined more tightly (Fig. 5c). The thickness of lithosphere is estimated to be  $\sim 600$ – $800 \text{ km}$  at present (Fig. 5d). These predictions (as a function of crustal thickness) may be considered as the most robust aspect of our modeling because they do not suffer

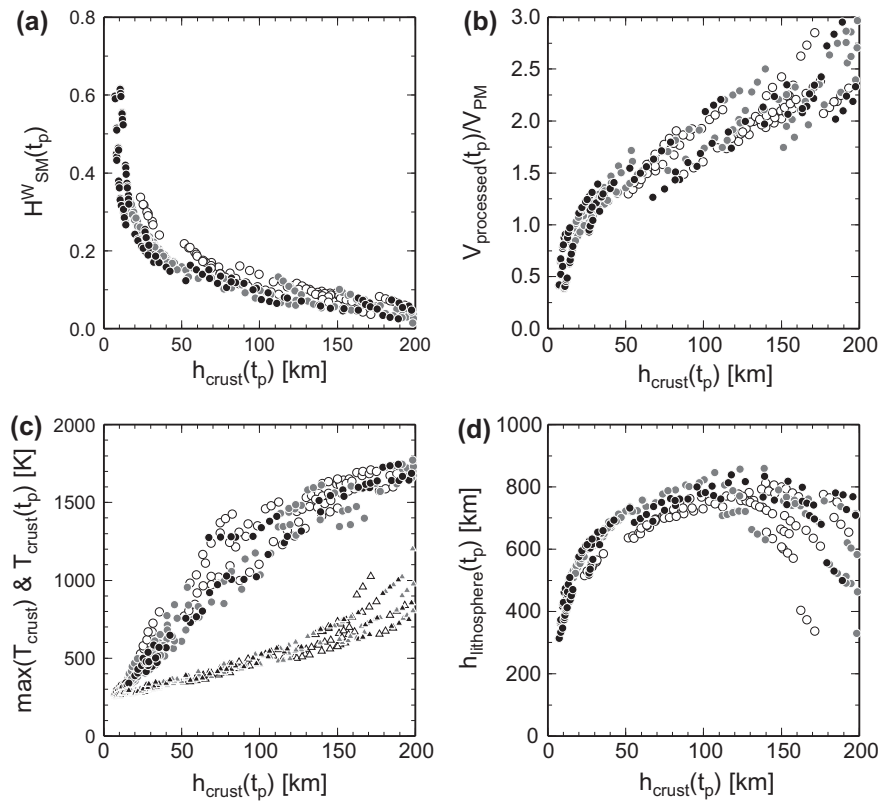


**Fig. 5.** Summary of all permutation runs, focusing on the results that are relatively insensitive to parameter uncertainty including dehydration stiffening. Open symbols denote cases with no dehydration stiffening ( $\Delta\mu$  of 1), whereas gray and solid symbols denote cases with  $\Delta\mu$  of 10 and 100, respectively. The number of all runs is 405, but those with predicted crustal thickness greater than 200 km are not shown here. (a) Normalized water concentration in the source mantle at present, (b) normalized volume of processed mantle at present, (c) maximum Moho temperature (circles) and present-day Moho temperature (triangles), and (d) thickness of thermal lithosphere at present. All are shown as a function of present-day crustal thickness.

from the uncertainty of free parameters such as the initial mantle temperature and the depth distribution of crustal heat production.

Note that at  $t = 0$ , there is no crust in our model, but the thickness of the stagnant lid is finite, so depleted mantle produced by any subsequent mantle melting would be added below this thin initial mantle lithosphere. As far as our modeling framework is concerned, therefore, we could expect the presence of primitive mantle right beneath the martian crust, but it is unrealistic given plausible planetary accretion scenarios, which involve the differentiation of shallow mantle by frequent impact melting. As the sensitivity test regarding the efficiency of mantle melting (i.e.,  $\gamma$ ) demonstrates, sublithospheric convection is always vigorous enough to convert all source mantle above the initial depth of melting to depleted mantle (Section 3.2 and Fig. 4). Also, the vast majority of permutation runs resulted in the processing the entire mantle at least once (Fig. 5b), indicating that the convective delamination of lithosphere usually takes place. So any primitive mantle preserved in the lithosphere, which may be better regarded as a modeling artifact, is likely to be diminished in most cases.

The effect of dehydration stiffening is mostly limited to the thermal aspects (Fig. 6), and we may simply summarize that dehydration stiffening tends to buffer planetary cooling, consistent to the preliminary scaling of Korenaga (2009b). Stiffer lithosphere leads to higher mantle temperature at present (Fig. 6a) as well as during the main melting phase (Fig. 6b). The difference in the predicted temperature caused by stiffening is as wide as  $\sim 400$  K. This spread is comparable to the range of initial mantle temperature (1550–1950 K), implying that the dehydration effect helps to retain the memory of initial conditions in the present-day mantle. The influence of dehydration stiffening is weaker on the present-day core temperature; i.e., greater  $\Delta\mu$  does not necessarily lead

to higher core temperature (Fig. 6c). The core temperature is more sensitive to the dynamics of the core–mantle boundary region, for which we assumed conventional scaling. Nonetheless, the temperature contrast at the core–mantle boundary, which drives convection in the core, can be considerably reduced in the presence of dehydration stiffening (Fig. 6d). The significance of these model systematics will be discussed next.

## 4. Discussion

### 4.1. Efficient degassing by stagnant-lid convection

Our thermal evolution model with mantle melting and crustal growth is built on the work of Hauck and Phillips (2002), which was the first coupled thermal–magmatic model that can reproduce the estimated crustal thickness as well as its formation history (i.e.,  $\sim 50$ – $100$  km of crust formed mostly by 4 Ga). As seen in Figs. 3 and 4, reproducing such crustal growth is possible for a range of model parameters. One major difference from Hauck and Phillips (2002) is the degree of dehydration in the mantle; their model predicts only 5–10% loss of the initial water in the mantle, whereas our study suggests more than 80% loss if the crust is thicker than  $\sim 50$  km (Fig. 5a). Though Hauck and Phillips (2002) used the distribution coefficient  $D$  of 0.1 when modeling the extraction of heat-producing elements from the mantle, they assumed  $D = 0$  for the extraction of water, which is the same as our formulation. The degree of mantle dehydration is mostly a simple function of crustal thickness and is not influenced much by the presence or absence of stiffening. The reason for this large discrepancy between Hauck and Phillips (2002) and our study is that we track the fate of residual mantle after melting (Section 2.3). When DML becomes thicker

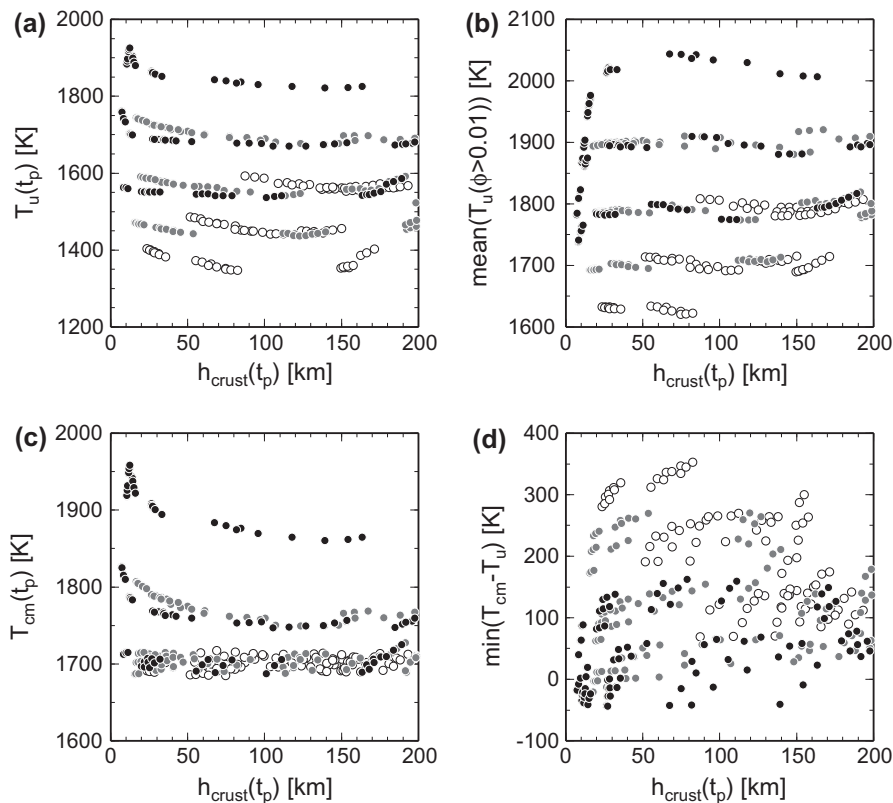


**Fig. 6.** Same as Fig. 5, but focusing on the results that are sensitive to the degree of dehydration stiffening. (a) Average mantle temperature at present, (b) time-averaged mantle temperature when the degree of melting  $\phi$  is greater than 0.01 (i.e., during major crustal growth), (c) core temperature at present, and (d) minimum temperature difference at the core–mantle boundary during the entire evolution. All are shown as a function of present-day crustal thickness.

than the predicted mantle lithosphere and convectively unstable, some lower fraction of DML is delaminated and mixed back into the source mantle (Eq. (20)), diluting its trace-element concentration. Treating lithospheric delamination is essential when calculating the evolution of trace-element budget of the source mantle in a self-consistent manner. It may be surprising that efficient degassing can be achieved even in the mode of stagnant-lid convection, but magma transport associated with crustal growth serves a pathway for degassing through the stagnant lid, and lithospheric delamination allows the mantle to be processed repeatedly by a small degree of melting.

The total abundance of water on Mars throughout its history remains one of the outstanding questions of martian geology (e.g., Jakosky and Phillips, 2001; Carr and Head, 2009), but our calculation of  $\sim 80\%$  degassing may at least provide a constraint on the total amount of water released from the mantle. The water concentration in our formulation is normalized by its initial concentration in the mantle, so in order to estimate the total amount of water degassed, we need to know the absolute water concentration in either the primitive or present-day mantle. The studies of the Chassigny meteorite yield potential water contents that range from 1 ppm (Mysen et al., 1998) to 1000 ppm (Johnson et al., 1991), and the study of the Shergottite meteorite source magma has led to predictions of up to 1.8 wt% water in the martian mantle (McSween et al., 2001). A detailed comparison of our results with these findings may not be very meaningful because the water concentration in the mantle can be spatially variable, and the martian meteorites could potentially tell us about only a small fraction of the source mantle. Instead we can turn to estimates of total initial mantle water content calculated from planetary accretion models. Lunine et al. (2003) suggested, for example, that water delivered by asteroids and comets during planetary accretion could provide a

source for Mars' water totaling 6–27% of Earth's present ocean, which is equivalent to 600–2700 m worth of water on the martian surface and regolith. If we use our estimate of  $\sim 80\%$  outgassing, approximately 500–2000 m equivalent of water would have been released from the mantle. This result is the same order of magnitude as geologic and geomorphic models that predict the total amount of water in the martian surface and crust ranged upwards of 500 m (Carr, 1987; Baker, 2001). However, there are uncertainties in both the accretion and geomorphic models, and our prediction of a relatively dry present-day martian mantle may be tested in the future by measuring the electrical conductivity of the mantle.

#### 4.2. Cold crustal evolution

The martian topography exhibits peculiar variations such as the hemispheric dichotomy and the Tharsis rise, which are estimated to have formed early in the evolution of Mars (e.g., Zuber et al., 2000; Phillips, 2001). The preservation of such topographic expression (and corresponding crustal thickness variation) on a billion-year time scale requires that the lower crust has never been hot enough to flow quickly (Zuber et al., 2000; Nimmo and Stevenson, 2001). This notion has been used to place a constraint on the crustal thickness (Nimmo and Stevenson, 2001) and on the style of surface cooling and mantle convection (Parmentier and Zuber, 2007). In particular, based on their thermal evolution model, Parmentier and Zuber (2007) suggested that either efficient cooling by hydrothermal circulation or inefficient mantle convection by compositional stratification is needed to preserve the ancient topographic variations if the crust is as thick as 50 km. The Moho temperature in their model (with a 50-km-thick crust) is quite high in the first 1 Gyr of the martian history, e.g.,  $\sim 1500$ – $1100$  K for the initial mantle temperature of 1773 K and  $\sim 1700$ – $1300$  K for the

initial temperature of 2073 K (see their Fig. 3). With the diabase rheology assumed for the lower crust, the Moho temperature must be lower than  $\sim 1100$  K for the relaxation rate to be sufficiently low ( $<10^{-17}$  s $^{-1}$ ) to maintain topographic variations. Some additional mechanism to cool down the crust thus seems to be required.

In contrast, the Moho temperature in our model does not get as high when the crustal thickness is  $\sim 50$  km (Fig. 5c). Even if the crust is as thick as  $\sim 100$  km, there are some parameter combinations that keep the maximum Moho temperature below 1100 K. This relatively cold crustal evolution is achieved in our study because crustal growth and mantle evolution are coupled. Conversely, in the model of [Parmentier and Zuber \(2007\)](#), crustal thickness was constant throughout the martian history and its growth by mantle melting was not considered. Also, a uniform distribution of crustal heat production was assumed, which results in higher Moho temperature than the exponential distribution (Fig. 4a). In our model, however, higher initial mantle temperature or more uniform crustal heat production results not only in higher Moho temperature, but also in thicker crust. Our modeling results suggest that, if the crust is too hot to preserve topographic variations, it would also be too thick to be consistent with the existing crustal thickness estimates. Although our study by itself does not preclude the possibility of hydrothermal cooling or a compositionally stratified mantle, we find that the preservation of ancient topographic features does not necessarily require them either.

#### 4.3. Insulated mantle?

As stated in Section 1, our primary objective was to study the effects of mantle melting such as dehydration stiffening and compositional buoyancy on the thermal evolution of Mars. Such melting effects, in particular dehydration stiffening, do indeed stabilize the top thermal boundary layer and suppress the heat flux from the mantle as well as its chemical differentiation (Fig. 3). Similar results can also be achieved by modifying other parameters such as the initial mantle temperature, the reference viscosity, and the depth distribution of crustal heat production (Fig. 4). Because of these parameter uncertainties, therefore, the effects of mantle melting are not readily visible in some aspects of modeling results (Fig. 5), and the impact of dehydration stiffening is mostly limited to modifying the relation between the crustal thickness and the mantle temperature (Fig. 6). For a crustal thickness of 50 km, for example, the present-day mantle temperature may be  $\sim 1400$ – $1500$  K without stiffening but could be higher than  $\sim 1800$  K if stiffening is significant (Fig. 6a). This large uncertainty in the present-day average mantle temperature may be important when interpreting subsurface geophysical properties such as seismic velocity and electrical conductivity.

The insulating effect of dehydration stiffening is also seen in the average mantle temperature during major crustal growth (Fig. 6b). For given crustal thickness, dehydration stiffening results in higher potential temperature of the source mantle, which in turn implies different crustal composition. The composition of the martian crust could thus be tightly related to the convective stability of the lithosphere, though we also need to better understand the petrology of the martian mantle at the same time (cf. [Agee and Draper, 2004](#)).

#### 4.4. Notes on core cooling and mantle plumes

The impact of dehydration stiffening is less direct on core cooling than on mantle cooling, because the former is controlled by the dynamics of the core–mantle boundary region and has little to do with the lithospheric stability. Except for some end-member cases, the core temperature is predicted to be  $\sim 1700$  K at present (Fig. 6c). This is because of the self-regulating nature of purely temperature-dependent viscosity assumed for the core–mantle

boundary region (Section 2.5). Higher core temperature lowers the viscosity of the boundary region, leading to higher core heat flux (i.e., efficient core cooling).

Because the core cannot cool faster than the mantle, however, inefficient mantle cooling by dehydration stiffening could result in non-monotonic core cooling (Figs. 3b and 6d) even with the conventional scaling for core heat flux. A thick DML in early Mars by dehydration stiffening can heat up the mantle sufficiently high to shut down the dynamo in the martian core. Based on thermal evolution modeling, the absence of the planetary-scale magnetic field has been used to constrain the amount of light elements in the core (e.g., [Schubert et al., 1992](#)), but we chose not to repeat this exercise in this study. As mentioned earlier, the rheology of the martian lower mantle is poorly known even if the martian mantle is compositionally similar to Earth's mantle. Higher core temperature may not always reduce the viscosity of the lowermost mantle ([Solomatov, 1996](#); [Korenaga, 2005](#)). The detailed understanding of the dynamics of the lowermost mantle is essential to utilize core-related observations in thermal evolution modeling, but it does not affect the first-order features of mantle evolution because core heat flux is generally much smaller than mantle heat flux (Fig. 3b).

For the same reason, we did not consider the possible contribution of mantle plumes from the core–mantle boundary to surface magmatism and thus crustal growth. Because core heat flux has been mostly positive in our model, its advective component is expected to manifest as mantle plumes. But the fraction of such advective component in the total core heat flux as well as the size and frequency of mantle plumes depend strongly on the rheology of the lowermost mantle ([Korenaga, 2005](#)). The consideration of plume contribution is nonetheless important to interpret the traces of volcanic activities on the surface of Mars.

## 5. Conclusions

The thermal evolution of terrestrial bodies is a complex process that is influenced by many variables. Varying even one of initial conditions or model parameters can have a large and sometimes unpredictable effect on the model outcome. We have constructed a new thermal evolution model that can take into account both crustal and lithospheric growth. The new scaling of [Korenaga \(2009b\)](#) allows us to model self-consistently the thermal and chemical evolution of the mantle, in particular the dynamics of the chemically depleted mantle, which is an unavoidable consequence of mantle melting and crustal growth. One of surprising yet robust results is the efficient processing and degassing of the mantle by stagnant-lid convection. Combined with the existing estimates on the thickness of the martian crust, the martian mantle is predicted to have lost its primordial water by  $>80\%$ . Water outgassed from the primitive mantle may have been voluminous enough to cover the planet with a global ocean many meters deep. The same degree of extraction applies to heat-producing elements, so most of mantle heat production has been sequestered in the crust. Dehydration stiffening upon mantle melting, if present, could substantially slow down mantle cooling, which in turn affect core cooling. As a result, the relations among crustal thickness, crustal composition, and temperature of the parental mantle become multi-valued, being strongly influenced by the initial mantle temperature. The interpretation of core-related observables such as the history of the martian magnetic field is suggested to require more care than previously given.

## Acknowledgments

This work was sponsored by the US National Science Foundation under Grant EAR-0449517 and by Microsoft A. Richard New-

ton Breakthrough Research Award. We thank David Bercovici for constructive comments on the earlier version of the manuscript. We also thank Editor Jim Bell and two anonymous reviewers for official reviews, which helped to improve the clarity of the paper.

## References

- Agee, C.B., Draper, D.S., 2004. Experimental constraints on the origin of martian meteorites and the composition of the martian mantle. *Earth Planet. Sci. Lett.* 224, 415–429.
- Baker, V.R., 2001. Water and the martian landscape. *Nature* 412, 228–236.
- Beattie, P., 1993. The effect of partial melting of spinel peridotite on uranium series disequilibria: Constraints from partitioning studies. *Earth Planet. Sci. Lett.* 177, 379–391.
- Bercovici, D., 2003. The generation of plate tectonics from mantle convection. *Earth Planet. Sci. Lett.* 205, 107–121.
- Bertka, C.M., Fei, Y., 1998. Density profile of an SNC model martian interior and the moment-of-inertia factor of Mars. *Earth Planet. Sci. Lett.* 157, 79–88.
- Bertka, C.M., Holloway, J.R., 1994. Anhydrous partial melting of an iron-rich mantle. I: Subsolidus phase assemblages and partial melting phase relations at 10 to 30 kbar. *Contrib. Mineral. Petrol.* 115, 313–322.
- Breuer, D., Spohn, T., 2003. Early plate tectonics versus single-plate tectonics on Mars: Evidence from magnetic field history and crust evolution. *J. Geophys. Res.* 108 (E7), 5072. doi:10.1029/2002JE001999.
- Carr, M.H., 1987. Water on Mars. *Nature* 326, 30–35.
- Carr, M.H., Head, J.W., 2009. Geologic history of Mars. *Earth Planet. Sci. Lett.* doi:10.1016/j.epsl.2009.06.042.
- Chopra, P.N., Paterson, M.S., 1984. The role of water in the deformation of dunite. *J. Geophys. Res.* 89, 7861–7876.
- Christensen, U., 1984. Convection with pressure- and temperature-dependent non-Newtonian rheology. *Geophys. J. R. Astron. Soc.* 77, 343–384.
- Connerney, J.E.P., Na, M.H.A., Wasilewski, P.J., Ness, N.F., Rème, H., Mazelle, C., Vignes, D., Lin, R.P., Mitchell, D.L., Cloutier, P.A., 1999. Magnetic lineation in the ancient crust of Mars. *Science* 284, 794–798.
- Davaille, A., Jaupart, C., 1994. Onset of thermal convection in fluids with temperature-dependent viscosity: Application to the oceanic mantle. *J. Geophys. Res.* 99, 19853–19866.
- Dreibus, G., Wänke, H., 1985. Mars, a volatile-rich planet. *Meteoritics* 20, 367–381.
- Fairén, A.G., Ruiz, J., Anguita, F., 2002. An origin for the linear magnetic anomalies on Mars through accretion of terranes: Implications for dynamo timing. *Icarus* 160, 220–223.
- Hager, B.H., 1991. Mantle viscosity: A comparison of models from postglacial rebound and from the geoid, plate driving forces, and advected heat flux. In: Sabadini, R., Lambeck, K., Boschi, E. (Eds.), *Glacial Isostasy, Sea-Level and Mantle Rheology*. Kluwer Academic, Dordrecht, pp. 493–513.
- Hart, S., Dunn, T., 1993. Experimental cpx/melt partitioning of 24 trace elements. *Contrib. Mineral. Petrol.* 113, 1–8.
- Hauck, S.A., Phillips, R.J., 2002. Thermal and crustal evolution of Mars. *J. Geophys. Res.* 107 (E7), 5052. doi:10.1029/2001JE001801.
- Hauri, E.H., Wagner, T.P., Grove, T.L., 1994. Experimental and natural partitioning of Th, U, Pb and other trace elements between garnet, clinopyroxene and basaltic melts. *Chem. Geol.* 117, 149–166.
- Herzberg, C., Asimow, P.D., Arndt, N., Niu, Y., Leshner, C.M., Fitton, J.G., Cheadle, M.J., Saunders, A.D., 2007. Temperatures in ambient mantle and plumes: Constraints from basalts, picrites, and komatiites. *Geochem. Geophys. Geosyst.* 8 (2), Q02206. doi:10.1029/2006GC001390.
- Hirschmann, M.M., 2000. Mantle solidus: Experimental constraints and the effects of peridotite composition. *Geochem. Geophys. Geosyst.* 1. doi:10.1029/2000GC000070.
- Hirschmann, M.M., Aubaud, C., Withers, A.C., 2005. Storage capacity of H<sub>2</sub>O in nominally anhydrous minerals in the upper mantle. *Earth Planet. Sci. Lett.* 236, 167–181.
- Hirth, G., Kohlstedt, D.L., 1996. Water in the oceanic mantle: Implications for rheology, melt extraction, and the evolution of the lithosphere. *Earth Planet. Sci. Lett.* 144, 93–108.
- Hirth, G., Kohlstedt, D., 2003. Rheology of the upper mantle and the mantle wedge: A view from the experimentalists. In: Eiler, J. (Ed.), *Inside the Subduction Factory*. American Geophysical Union, Washington, DC, pp. 83–105.
- Jakosky, B.M., Phillips, R.J., 2001. Mars' volatile and climate history. *Nature* 412, 237–244.
- Jaupart, C., Mareschal, J.-C., 2003. Constraints on crustal heat production from heat flow data. In: Holland, H., Turekian, K.K. (Eds.), *Treatise on Geochemistry*, vol. 3. Elsevier, pp. 65–84.
- Johnson, M.C., Rutherford, M.J., Hess, P.C., 1991. Chassigny petrogenesis: Melt compositions, intensive parameters, and water contents of martian (?) magmas. *Geochim. Cosmochim. Acta* 55, 349–366.
- Karato, S., Wu, P., 1993. Rheology of the upper mantle: A synthesis. *Science* 260, 771–778.
- Karato, S., Paterson, M.S., FitzGerald, J.D., 1986. Rheology of synthetic olivine aggregates: Influence of grain size and water. *J. Geophys. Res.* 91, 8151–8176.
- Kelemen, P.B., Holbrook, W.S., 1995. Origin of thick, high-velocity igneous crust along the US East Coast Margin. *J. Geophys. Res.* 100, 10077–10094.
- Khan, A., Connolly, J.A.D., 2008. Constraining the composition and thermal state of Mars from inversion of geophysical data. *J. Geophys. Res.* 113, E07003. doi:10.1029/2007JE002996.
- Kinzler, R.J., Grove, T.L., 1992. Primary magmas of mid-ocean ridge basalts, 2, applications. *J. Geophys. Res.* 97 (B5), 6907–6926.
- Koga, K., Hauri, E., Hirschmann, M., Bell, D., 2003. Hydrogen concentration analysis using SIMS and FTIR: Comparison and calibration for nominally anhydrous minerals. *Geochem. Geophys. Geosyst.* 4, 1019. doi:10.1029/2002GC000378.
- Korenaga, J., 2003. Energetics of mantle convection and the fate of fossil heat. *Geophys. Res. Lett.* 30 (8), 1437. doi:10.1029/2003GL016982.
- Korenaga, J., 2005. Firm mantle plumes and the nature of the core–mantle boundary region. *Earth Planet. Sci. Lett.* 232, 29–37.
- Korenaga, J., 2006. Archean geodynamics and the thermal evolution of Earth. In: Benn, K., Mareschal, J.-C., Condie, K. (Eds.), *Archean Geodynamics and Environments*. American Geophysical Union, Washington, DC, pp. 7–32.
- Korenaga, J., 2007. Thermal cracking and the deep hydration of oceanic lithosphere: A key to the generation of plate tectonics? *J. Geophys. Res.* 112, B05408. doi:10.1029/2006JB004502.
- Korenaga, J., 2008. Plate tectonics, flood basalts, and the evolution of Earth's oceans. *Terra Nova* 20, 419–439.
- Korenaga, J., 2009a. How does small-scale convection manifest in surface heat flux? *Earth Planet. Sci. Lett.* 287, 329–332.
- Korenaga, J., 2009b. Scaling of stagnant-lid convection with Arrhenius rheology and the effects of mantle melting. *Geophys. J. Int.* 179, 154–170.
- Korenaga, J., Jordan, T.H., 2002a. On 'steady-state' heat flow and the rheology of oceanic mantle. *Geophys. Res. Lett.* 29 (22), 2056. doi:10.1029/2002GL016085.
- Korenaga, J., Jordan, T.H., 2002b. Onset of convection with temperature- and depth-dependent viscosity. *Geophys. Res. Lett.* 29 (19), 1923. doi:10.1029/2002GL015672.
- Korenaga, J., Kelemen, P.B., Holbrook, W.S., 2002c. Methods for resolving the origin of large igneous provinces from crustal seismology. *J. Geophys. Res.* 107 (B9), 2178. doi:10.1029/2001JB001030.
- Korenaga, J., Karato, S., 2008. A new analysis of experimental data on olivine rheology. *J. Geophys. Res.* 113, B02403. doi:10.1029/2007JB005100.
- Lachenbruch, A.H., 1970. Crustal temperature and heat production – Implications of linear heat-flow relation. *J. Geophys. Res.* 75, 3291–3300.
- Langmuir, C.H., Klein, E.M., Plank, T., 1992. Petrological systematics of mid-ocean ridge basalts: Constraints on melt generation beneath ocean ridges. In: Phipps Morgan, J., Blackman, D.K., Sinton, J.M. (Eds.), *Mantle Flow and Melt Generation at Mid-Ocean Ridges*. Geophys. Monogr. Ser., vol. 71. AGU, Washington, DC, pp. 183–280.
- Lee, C.-T.A., 2004. Compositional variation of density and seismic velocities in natural peridotites at STP conditions: Implications for seismic imaging of compositional heterogeneities in the upper mantle. *J. Geophys. Res.* 108, 2441. doi:10.1029/2003JB002413.
- Lodders, K., Fegley, B., 1997. An oxygen isotope model for the composition of Mars. *Icarus* 126, 373–394.
- Lunine, J.I., Chambers, J., Morbidelli, A., Leshin, L.A., 2003. The origin of water on Mars. *Icarus* 165, 1–8.
- Lyubetskaya, T., Korenaga, J., 2007. Chemical composition of Earth's primitive mantle and its variance, 1, methods and results. *J. Geophys. Res.* 112, B03211. doi:10.1029/2005JB004223.
- Marinova, M.M., Aharonson, O., Asphaug, E., 2008. Mega-impact formation of the Mars hemispheric dichotomy. *Nature* 453, 1216–1219.
- McDonough, W.F., Sun, S.-S., 1995. The composition of the Earth. *Chem. Geol.* 120, 223–253.
- McGovern, P.J., Solomon, S.C., Smith, D.E., Zuber, M.T., Simons, M., Wiczorek, M.A., Phillips, R.J., Neumann, G.A., Aharonson, O., Head, J.W., 2002. Localized gravity/topography admittance and correlation spectra on Mars: Implications for regional and global evolution. *J. Geophys. Res.* 107, 5136. doi:10.1029/2002JE001854.
- McKenzie, D., Bickle, M.J., 1988. The volume and composition of melt generated by extension of the lithosphere. *J. Petrol.* 29, 625–679.
- McSween, H.Y., Grove, T.L., Lentz, R.C.F., Dann, J.C., Holzheid, A.H., Riciputi, L.R., Ryan, J.G., 2001. Geochemical evidence for magmatic water within Mars from pyroxenes in the Shergotty meteorites. *Nature* 409, 487–490.
- Mei, S., Kohlstedt, D.L., 2000a. Influence of water on plastic deformation of olivine aggregates, 1, diffusion creep regime. *J. Geophys. Res.* 105, 21457–21469.
- Mei, S., Kohlstedt, D.L., 2000b. Influence of water on plastic deformation of olivine aggregates, 2, dislocation creep regime. *J. Geophys. Res.* 105, 21471–21481.
- Mysen, B.O., Virgo, D., Popp, R.K., Bertka, C.M., 1998. The role of H<sub>2</sub>O in martian magmatic systems. *Am. Mineral.* 83, 942–946.
- Nimmo, F., Stevenson, D.J., 2000. Influence of early plate tectonics on the thermal evolution and magnetic field of Mars. *J. Geophys. Res.* 105 (E5), 11969–11979.
- Nimmo, F., Stevenson, D.J., 2001. Estimates of martian crustal thickness from viscous relaxation of topography crustal thickness from viscous relaxation of topography. *J. Geophys. Res.* 106 (E3), 5085–5098.
- Nimmo, F., Hart, S.D., Korycansky, D.G., Agnor, C.B., 2008. Implications of an impact origin for the martian hemispheric dichotomy. *Nature* 453, 1220–1223.
- Parmentier, E.M., Hess, P.C., 1992. Chemical differentiation of a convecting planetary interior: Consequences for a one plate planet such as Venus. *Geophys. Res. Lett.* 19, 2015–2018.
- Parmentier, E.M., Zuber, M.T., 2007. Early evolution of Mars with mantle compositional stratification or hydrothermal crustal cooling. *J. Geophys. Res.* 112, E02007. doi:10.1029/2005JE002626.

- Phillips, R.J., 2001. Ancient geodynamics and global-scale hydrology on Mars. *Science* 291, 2587–2591.
- Phillips, R.J., Malin, M.C., 1983. The interior of Venus and tectonic implications. In: Venus. University of Arizona Press, pp. 159–214.
- Reese, C.C., Solomatov, V.S., Moresi, L.-N., 1998. Heat transport efficiency for stagnant lid convection with dislocation viscosity: Application to Mars and Venus. *J. Geophys. Res.* 103 (E6), 13643–13657.
- Sanloup, C., Jambon, A., Gillet, P., 1999. A simple chondritic model of Mars. *Phys. Earth Planet. Int.* 112, 43–54.
- Schubert, G., Solomon, S.C., Turcotte, D.L., Drake, M.J., Sleep, N.H., 1992. Origin and thermal evolution of Mars. In: Kieffer, H.H., Jakosky, B.M., Snyder, C.W., Matthews, M.S. (Eds.), Mars. University of Arizona Press, Tucson, AZ, pp. 147–183.
- Schubert, G., Turcotte, D.L., Olson, P., 2001. Mantle Convection in the Earth and Planets. Cambridge, New York.
- Shaw, D.M., 1970. Trace element fractionation during anatexis. *Geochim. Cosmochim. Acta* 34, 237–243.
- Sleep, N.H., 1994. Martian plate tectonics. *J. Geophys. Res.* 99, 5639–5655.
- Solomatov, V.S., 1995. Scaling of temperature- and stress-dependent viscosity convection. *Phys. Fluids* 7, 266–274.
- Solomatov, V.S., 1996. Can hotter mantle have a larger viscosity? *Geophys. Res. Lett.* 23, 937–940.
- Solomatov, V.S., Moresi, L.-N., 1996. Stagnant lid convection on Venus. *J. Geophys. Res.* 101 (E2), 4737–4753.
- Solomatov, V.S., Moresi, L.-N., 2000. Scaling of time-dependent stagnant lid convection: Application to small-scale convection on Earth and other terrestrial planets. *J. Geophys. Res.* 105, 21795–21817.
- Spohn, T., 1991. Mantle differentiation and thermal evolution of Mars, Mercury, and Venus. *Icarus* 90, 222–236.
- Stevenson, D.J., Spohn, T., Schubert, G., 1983. Magnetism and thermal evolution of the terrestrial planets. *Icarus* 54, 466–489.
- Takahashi, E., Kushiro, I., 1983. Melting of a dry peridotite at high pressures and basalt magma genesis. *Am. Mineral.* 68, 859–879.
- Turcotte, D.L., Schubert, G., 1982. Geodynamics: Applications of Continuum Physics to Geological Problems. John Wiley, New York.
- Walter, M.J., 1998. Melting of garnet peridotite and the origin of komatiite and depleted lithosphere. *J. Petrol.* 39, 29–60.
- Wänke, H., Dreibus, G., 1994. Chemistry and accretion of Mars. *Philos. Trans. R. Soc. London A* 349, 2134–2137.
- Watts, A.B., Zhong, S., 2000. Observations of flexure and the rheology of oceanic lithosphere. *Geophys. J. Int.* 142, 855–875.
- Wieczorek, M.A., Zuber, M.T., 2004. Thickness of the martian crust: Improved constraints from geoid-to-topography ratios. *J. Geophys. Res.* 109, E01009. doi:10.1029/2003JE002153.
- Zuber, M.T., 2001. The crust and mantle of Mars. *Nature* 412, 220–227.
- Zuber, M.T., and 14 colleagues, 2000. Internal structure and early thermal evolution of Mars from Mars Global Surveyor topography and gravity. *Science* 287, 1788–1793.